[Frontiers in Bioscience 13, 5732-5754, May 1, 2008]

# *In vitro* assays of molecular motors – impact of motor-surface interactions

**Alf Mansson[1], Martina Balaz[1], Nuria Albet-Torres[1], K. Johan Rosengren[1]**

[1]*School of Pure and Applied Natural Sciences, University of Kalmar, SE-391 82 Kalmar, Sweden*

**TABLE OF CONTENTS**



## 1. ABSTRACT

In many types of biophysical studies of both single molecules and ensembles of molecular motors the motors are adsorbed to artificial surfaces. Some of the most important assay systems of this type (*in vitro* motility assays and related single molecule techniques) will be briefly described together with an account of breakthroughs in the understanding of actomyosin function that have resulted from their use. A poorly characterized, but potentially important, entity in these studies is the mechanism of motor adsorption to surfaces and the effects of motor surface interactions on experimental results. A better understanding of these phenomena is also important for the development of commercially viable nanotechnological applications powered by molecular motors. Here, we will consider several aspects of motor surface interactions with a particular focus on heavy meromyosin (HMM) from skeletal muscle. These aspects will be related to heavy meromyosin structure and relevant parts of the vast literature on protein-surface interactions for non-motor proteins. An overview of methods for studying motor-surface interactions will also be given. The information is used as a basis for further development of a model for HMM-surface interactions and is discussed in relation to experiments where nanopatterning has been employed for *in vitro* reconstruction of actomyosin order. The challenges and potentials of this approach in biophysical studies, compared to the use of self-assembly of biological components into supramolecular protein aggregates (*e.g.* myosin filaments) will be considered. Finally, this review will consider the implications for further developments of motor-powered lab-on-a-chip devices.

## 2. INTRODUCTION

### 2.1. General

The molecular motors are cellular nano-machines that convert chemical free energy in the form of high-energy phosphates into mechanical work (1; 2). There are three main classes of linear molecular motors that interact with cytoskeletal filaments (actin filaments or microtubules) to produce force or motility or to transport cargoes. The different classes are the dyneins and kinesins that walk along microtubule tracks and the myosins that walk along, or translocate actin filaments.

The present review will consider biophysical assays and nanotechnological applications where molecular motors are adsorbed to surfaces. Particular emphasis will be given to the importance of surface-motor interactions in these assays. In order to limit the scope of the review we will focus on myosin motors, in particular the proteolytic motor fragment heavy meromyosin (HMM) of skeletal muscle myosin II. Some aspects of surface-motor interactions for the kinesin-microtubule system (3-6) have been recently reviewed (7) and discussed in comparison to the actomyosin system elsewhere (8).

For surface-immobilization of proteins, whether these are antibodies in *e.g.* biosensor systems or molecular motors in biophysical assays, it is important with: 1. correct orientation for optimal function and 2. sufficiently strong immobilization to prevent rapid detachment from the surface while, simultaneously, not triggering excessive conformational changes. These goals can be achieved in different ways (9; 10). One possibility is direct covalent coupling between functionalities on the surface and specific amino-acids on the protein. Alternatively, affinity coupling molecules, such as antibodies (11) or the biotin-streptavidin system (12), may be used. One part of these coupling molecules then bind non-covalently to a specific region on the protein while another part is appropriately immobilized on a surface. Whereas surface immobilization via specific residues has potential advantages, it is associated with increased level of complexity compared to physical adsorption. Accordingly, the latter method is by far the most common for immobilization of molecular motors in both biophysical studies and nanotechnological applications. For this and other reasons, the present review will focus on non-specific physical adsorption of motors.

### 2.2. Why is insight into motor-surface interactions important?

Biophysical assay systems that rely on immobilization of motors to artificial surfaces include *in vitro* motility assays (13) and related single molecule assays (14). In a majority of the studies using such systems, the experiments have been performed without detailed considerations of motor-surface interactions. Only more recently has the interest to understand these phenomena grown considerably, driven by efforts to exploit molecular motors in nanotechnological applications (reviewed in (15-17)). In such applications, it is important with the selective localization of motor function to nano-sized tracks with suppression of motor function and motility in surrounding regions. The effectiveness of achieving selectivity by various methods of chemical surface patterning (Figure 1) has clearly demonstrated the critical dependence of motor function on the underlying surface properties.

Whereas early efforts to achieve selective localization of motor function on a chip were largely by trial and error, there has been growing insight that in depth understanding of the adsorption mechanisms are required for optimization of the system. This is essential in order to achieve robust and high-quality motor function for production of commercially viable nano-devices (16; 18). Moreover, it is of interest to create systems where motility may be reversibly switched on and off locally by changes, either in motor (19) or surface properties (20). If successful, such attempts will be of importance in nanotechnology but may also contribute to further insights into motor regulation in living cells (21; 22) as well as into protein biophysics in general (*cf.* (23)).

A detailed understanding of surface-motor interactions in different experimental systems will also be important for the interpretation of experimental results in biophysical assays as well as correct extrapolation of such results to *in vivo* motor properties (*cf.* (24) ).

Finally, studies of motor-surface interactions will contribute to the understanding of surface-protein interactions in general, a field of immense importance in biotechnology (10; 23; 25; 26). Relevant applications involve non-fouling surfaces, biomaterials, biosensors and specific protein immobilization in high throughput drug-discovery devices. The special properties of motors make them interesting model proteins for such studies of general mechanisms (*cf.* (8)). For instance, the highly asymmetric motors have regions of varying chemistry with respect to charge and conformational flexibility and may be useful as critical test proteins for evaluating the effectiveness of non-fouling, protein-resistant surfaces.

## 3. *IN VITRO* MOTILITY ASSAYS AND OPTICAL TWEEZERS EXPERIMENTS

*In vitro* motility assays (IVMA) are performed in two major configurations. In the first version, motor-coated beads are observed as they are transported along oriented arrays of actin filaments or microtubules that are immobilized on a surface (27; 28). In the second, and most common version (the gliding motility assay; (13; 29)), fluorescent cytoskeletal filaments are observed as they are transported by randomly oriented surface immobilized motors (Figure 2). The assay differs in details when applied to different motor systems (30). Here, we focus on the gliding configuration with myosin II or its proteolytic fragments subfragment 1 (S1) or heavy meromyosin (HMM) adsorbed to surfaces. Conventionally, nitrocellulose films are used as substrate for protein adsorption but different silanized surfaces and polymers have also been used (see further below).

Details regarding the general incubation steps for IVMAs vary slightly between labs but the principles are

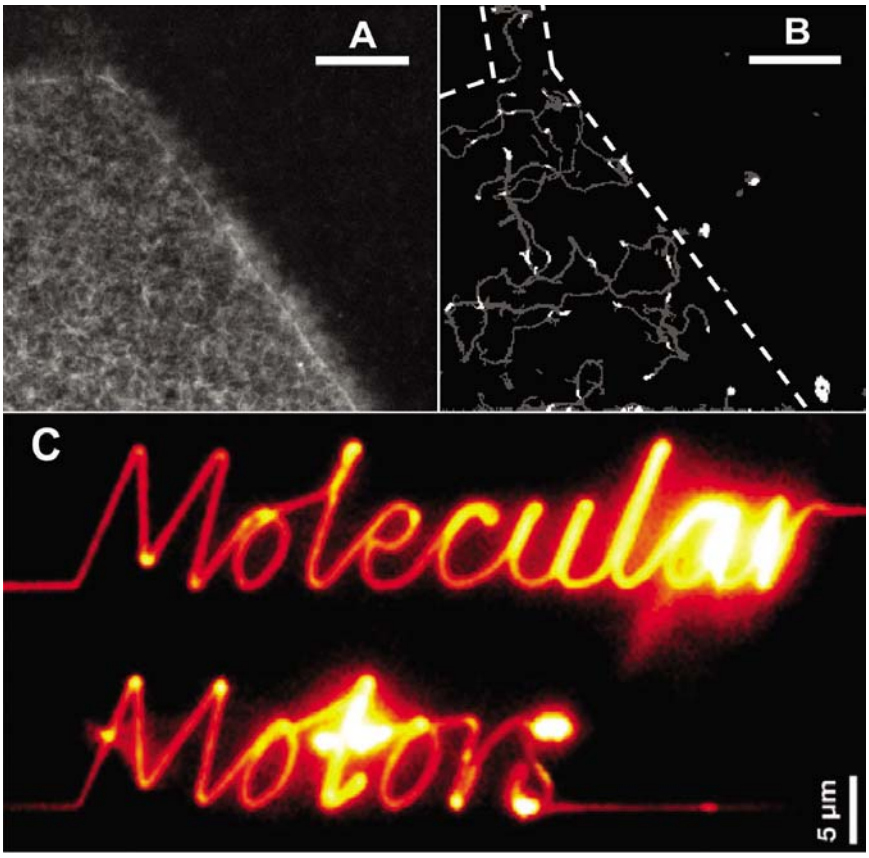


**Figure 1.** High-quality actomyosin motor function selectively localized to certain regions on micro-patterned (A and B) and nano-patterned surface (C). (A) Micro-patterned surface with pure $SiO_2$ area to the right (dark) and silanized, hydrophobic area to the left (bright due to binding of Alexa-488-phalloidin labelled actin filaments to HMM). Entire surface pre-incubated with HMM at a concentration of 130 micrograms $ml^{-1}$ for 2 min. Scale bar 15 micrometers, temperature 18 °C. (B) Same surface as in part A but after exchange of fluorescence filter set for the observation of individual rhodamine-phalloidin labelled actin filaments added at low concentration. Sum of 90 fluorescence images (0.5. s exposures) show filament trajectories. Positions of filaments indicated by bright time markers every 12 s. Border between TMCS and $SiO_2$ indicated by dashed lines. (C) Time-integrated image sequence (45 frames, 7.5. fps) of fluorescent actin filaments moving in a channel structure whose geometries permit only straight, forward motion (200 nm bottom channel width with silanized surface). This resulted in the text 'Molecular Motors' being spelled out, sequentially. Artificial coloring of the light intensity from red (lowest) to white (highest) applied after optimization of the image contrast. The areas surrounding the channels for guiding of the motors consisted of polymethylmethacrylate (PMMA) made hydrophilic by treatment with oxygen plasma. Scalebar in C, 5 micrometers. Assay solutions in A-C without methylcellulose and with an ionic strength of 40 mM. Figures in A and B reprinted with permission, from (34). Copyright (2006) American Chemical Society. Figure in C reprinted from (111) with permission from IOP Publishing Limited.

similar (31-33). Briefly, incubation with the motors or motor fragments is followed by blocking with *e.g.* bovine serum albumin (BSA; to block non-coated surface sites) and, usually, with unlabelled actin ((31; 33); to block non-functional rigor-like heads). Finally, the flow cell is incubated with fluorescent actin filaments and MgATP containing assay solution. The assay solution may contain methylcellulose to prevent diffusion of the actin filaments away from the surface at low motor density and/or high ionic strength. The duration of the HMM incubation step can vary slightly (1 – 2 min) but this is probably not an important source of variation between labs considering the apparently fast time course of HMM adsorption (*cf.* Figure 3; (34)).

The *in vitro* motility assay was early extended to allow measurement of inter-molecular forces. Originally, this was achieved by attachment of actin filaments to glass microneedles with the possibility to record force producing events attributed to a limited number of actomyosin interactions (35). However, in the early and mid nineties optical tweezers systems were implemented for measuring pN forces and nm displacements, generated in single actin-myosin interactions (14; 36). In the three-bead geometry (Figure 4), used in a vast majority of these studies (reviewed in (31; 37; 38)), an actin filament is suspended between two beads held in optical traps. The myosin motors or their motor fragments are immobilized at very low density on a third bead, or on a microfabricated

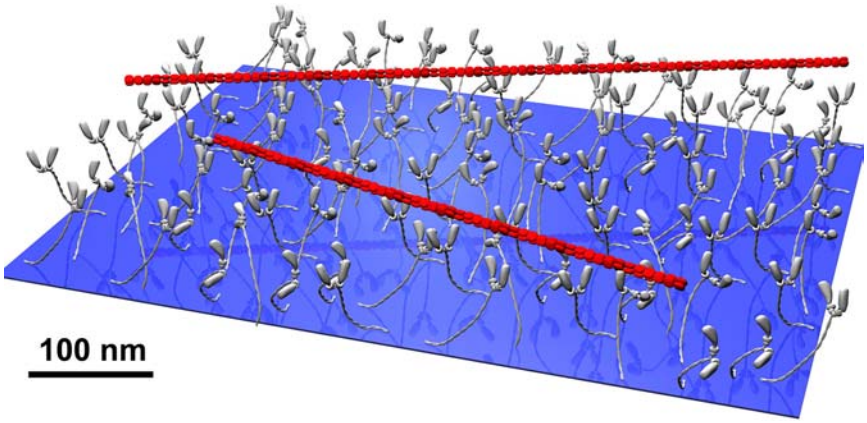


**Figure 2.** Principle for gliding *in vitro* motility assay where HMM molecules (gray), that are immobilized on a suitable surface substrate, propel actin filaments (red) upon addition of a suitable ATP containing buffer solution.

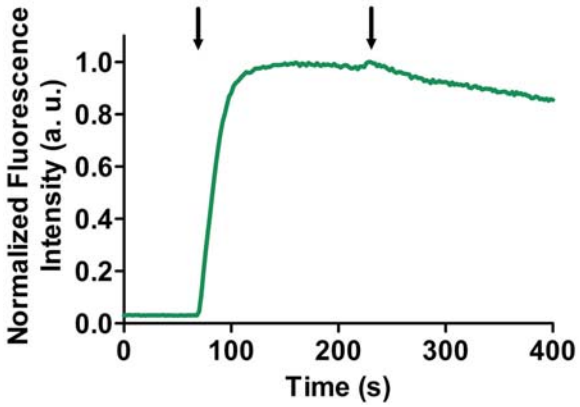


**Figure 3.** Total internal reflection fluorescence (TIRF) spectroscopy data showing the time course of HMM adsorption on a TMCS coated fused silica ($SiO_2$) TIRF slide. HMM infusion (130 micrograms $ml^{-1}$) started at the first arrow, was terminated after 40 s and then followed by rinsing with wash solution at the second arrow. Proteins were subjected to evanescent wave excitation at 280 nm and fluorescence emission was measured at 335 nm. Data normalized to maximum value. Note negligible bulk contribution due to HMM in solution and desorption of the HMM upon rinsing with protein free solution. Small excitation slit used, making effects of photobleaching negligible.

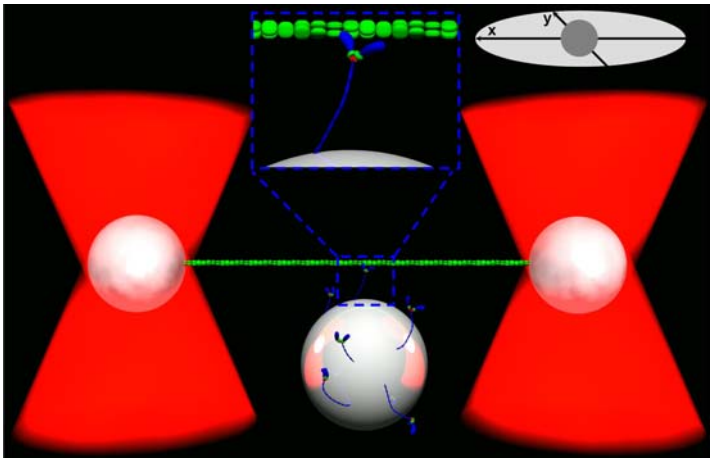


**Figure 4.** Schematic illustration of optical tweezers experiment in the three-bead geometry. The actin filaments are bound to beads held in traps of focused laser beams. The motors are immobilized at low density on a third bead (in the middle) placed on a cover slip. Upon lowering of the actin filament towards the bead with motors random binding events, and associated forces and displacements, may be detected by monitoring the position of one, or both, trapped beads by means of optical quadrant detectors.

**Table 1.** Important developments or results obtained by *in vitro* motility assays or optical tweezers experiments[1]

| Year | Development/Result | Refs |
|---|---|---|
| 1983-1985 | First motility assays with the bead geometry. | (27; 28) |
| 1984 | Observation of single fluorescent actin filaments in epifluorescence | (157) |
| 1986 | First gliding motility assay | (29) |
| 1987-1988 | One-headed myosin and subfragment 1 sufficient to produce force and to propel actin filaments | (35; 158; 159) |
| 1989, 1997 | Actin filament polarity determines sliding direction. Myosin propels actin independent of orientation | (56; 160) |
| 1990-1991 | *In vitro* motility assays at low motor density and with very short actin filaments for estimation of duty ratio and step length | (32; 115; 161) |
| 1992 | Similarity and differences between *in vitro* motility assays and fibre experiments in effects of several experimental parameters. Improvement of tracking algorithms and motility assay procedure. | (33) |
| 1993 | Right handed rotation of actin filament during *in vitro* sliding | (162) |
| 1994 | First optical tweezers studies in three-bead geometry and first single molecule force measurements on actomyosin | (14) |
| 1995 | Improved methods for determination of step length and on-time and first measurement of step length (4 nm) from a single myosin head (S1) | (36) |
| 1996 | Bead-tailed actin filament – of importance in optical tweezers studies and for nanotechnology. Estimation of torque exerted by myosin on actin | (163) |
| 1997 | First *in vitro* motility assay using surfaces micropatterned by UV-lithography | (100) |
| 1998 | Simultaneous observation of mechanical and chemical events in actomyosin by optical tweezers studies and single molecule fluorescence | (12) |
| 1999 | Two heads are better than one in force-generation | (41) |
| 1999 | Two-step force generation observed in myosin I but not in myosin II | (42) |
| 1999-2000 | Studies of myosin (with single isoform) isolated from single muscle fibres using slightly different approaches | (50-52) |
| 2001 | Optical tweezers experiments used to map "target zones" of favorably oriented sites on the helices of the actin filament | (40) |
| 1990-2003 | Several *in vitro* motility assay studies of activation mechanism using thin filaments reconstituted in different ways | (32; 46; 57; 62; 164) |
| 2003 | First actomyosin *in vitro* motility assay using surface nanostructured by E-beam lithography | (102) |
| 2003 | Load dependent kinetics of force production in smooth muscle myosin demonstrated by a new optical tweezers based technique | (165) |
| 2004 | "Backwards motility" *in vitro* produced by engineering an originally "forward directed" plus end motor | (166) |
| 2006 | Optical tweezers studies demonstrate two-step force generation by myosin II | (39) |

[1]The list is non-exhaustive and is strongly focused on myosin II of muscle

pedestal (12), placed on a cover-slip surface. To initiate actomyosin interactions the actin filaments are brought in close proximity to the bead or the pedestal. Motor-induced forces or displacements may then be detected by tracking the position of the trapped beads using a quadrant photo-detector.

In these single molecule experiments the surfaces with the beads are incubated with generally similar buffer solutions as in motility assays but with considerably lower motor concentration and usually a very low MgATP concentration. The immobilization of HMM, S1 and myosin are generally achieved by non-specific adsorption to nitrocellulose coated beads (14; 36; 39-43). However, specific immobilization *e.g.* via antibodies (41) has also been utilized for subfragment 1 and immobilization via His-tags has been exploited for engineered myosin constructs (44). Furthermore, thick filaments have been immobilized on pedestals with myosin heads extending from their backbone (12; 45).

*In vitro* motility assays and optical tweezers studies have contributed immensely to the understanding of molecular motor function (*e.g.* summarized in (1; 37; 38; 46)). A non-exhaustive list of important results with focus on myosin II is given in Table 1.

In spite of the success and general usefulness of the *in vitro* motility assays and related single molecule techniques there are a number of issues that need to be further considered for both nanotechnological applications (16; 17; 47) and biophysical studies (24; 48; 49). For nanotechnological applications one main concern is the limited life-time of the motors in a device situation. For biophysical assays this issue is not of any major relevance. However, it is clear that there are a number of apparent discrepancies between the IVMA studies and optical tweezers studies on one hand and theoretical predictions and the *in vivo* behavior of the motors on the other. For instance, using HMM, Homsher *et al* (33) found differences in ionic strength-, pH- and temperature dependence of sliding velocity compared to the situation in fibers. Moreover, by isolating myosin from single muscle fibres (50; 51) unloaded fibre shortening speed could be directly compared to the *in vitro* motility assay sliding velocity, with markedly lower velocity in the latter case. Whereas Hook *et al* (52) did not note the same discrepancy in their elegant single fibre motility assay, the effect was later observed again using *in vitro* motility assays with synthetic myosin filaments that contained well-defined myosin heavy chain isoforms (49).

As regards optical tweezers studies one uncertainty is the myosin step length. Usually a step length of about 5 nm has been observed (*e.g.* (36; 39; 40). However, in several studies (14; 41; 45) with two-headed myosin constructs, or with one-headed myosin molecules in myosin-rod co-filaments at "appropriate" orientation, a value close to 10 nm was observed. This is more consistent with X-ray crystallographic data (53; 54) and X-ray interference experiments in muscle fibers (55).

The observed differences between the *in vitro* motility assay and optical tweezers results on one hand, and theoretical predictions and experimental results obtained using muscle fibers on the other, can be attributed to a combination of several factors. These include the loss of *in vivo* order in the *in vitro* experiments (24; 45; 49; 56), changes in supramolecular composition (*e.g.* loss of troponin and tropomyosin; (32; 46; 57)), differences in

buffer composition (58; 59) , limitations in analysis methods or models (60; 61) *etc*. In addition (see further (24)) it is clear from Figure 1 that surface motor interactions may have significant effects on function (see also Figure 7 below). Furthermore, it has been shown that the relationship between pH and sliding velocity exhibits differences when HMM is adsorbed on nitrocellulose and on a silanized surface (24). Finally, the mechanism of $Ca^{2+}$ activation of reconstituted thin filaments seems to be different on nitrocellulose and silanized surfaces (46; 62). As further discussed below, some of the effects of different surface chemistries may be attributed to different configurations (orientations) of the HMM molecules.

## 4. MECHANISMS OF PROTEIN ADSORPTION

The great significance of surface-adsorption of proteins in various applications, has motivated a vast number of studies of the underlying mechanisms (reviewed in (10; 23; 25; 26)). Due to the complexity there is still no detailed theory that allows accurate predictions of adsorption behavior. However, a general picture that has emerged is that the driving forces for adsorption are mainly electrostatic and entropic in nature with minor relevance of van der Waals interactions.

The importance of electrostatic interactions was strikingly demonstrated by the major effects on adsorption kinetics resulting from the exchange of a single charged amino acid residue in cytochrome $b_5$ (63). In addition to the obvious effects of charge density and sign, and their dependence on pH, several other factors determine the strength of electrostatic protein-surface interactions. One of the most important is the well-known decrease in electrostatic interactions with increased ionic strength. In depth insight has been gained through model simulations (64) considering proteins of low surface coverage and their electrostatic and van der Waals interaction energies with the surface. In these simulations, the equilibrium constant for protein adsorption to a surface of opposite charge was reduced by up to 1-2 orders of magnitude by increasing the ionic strength from 0 to 100 mM. However, also at 100 mM, the equilibrium constant was up to several orders of magnitude (depending on assumed surface and protein charge) higher on charged surfaces than in the absence of surface or protein charge. The persistent importance of electrostatic interactions in adsorption phenomena up to, and above, physiological ionic strengths has been confirmed in experimental studies (65). Moreover, the relevance of electrostatic interactions under these conditions is also clear from their importance in the actomyosin interaction (2; 66-71).

Even if proteins have zero net charge there may be strong electrostatic interactions between the surfaces and certain protein domains or loops, particularly if the proteins are strong electric dipoles. Such effects may determine surface orientation as clearly demonstrated in a series of theoretical and experimental studies of antibodies at positively and negatively charged surfaces (72-74). On the basis of a residue-based protein-surface interaction potential model and Monte Carlo simulations Zhou *et al* (73) suggested that electrostatic and van der Waals interactions co-determine the orientation of the adsorbed antibodies. At ionic strengths up to about 100 mM (depending on the dipole moment and surface charge) the simulations suggested predominance of electrostatic interactions with noticeable effects of charge density and sign on antibody orientation. The preferred orientations of antibodies on charged surfaces, was later confirmed experimentally (72; 74). In this connection, it is of interest to note that the antibodies in the referenced studies exhibited dipole moments (1400 – 3200 D) that are in the same range as for relevant myosin motor fragments (see below).

Regarding entropic interactions these include conformational entropy and hydrophobic interactions. The latter result from the increase in entropy of the water molecules (smaller total area of structured water) as hydrophobic regions of the proteins are brought in direct contact with a hydrophobic surface. This effect increases with temperature and, in contrast to electrostatic interactions, also with ionic strength. Its magnitude is strongly dependent on the specific salt, and it is the basis for "salting out" effects and hydrophobic interaction chromatography. In consistence with these effects, increased adsorption of proteins on hydrophobic surfaces may be expected with increased ionic strength or temperature.

The conformational entropy as a driving force for adsorption varies for proteins depending on their internal structural stability (25). Thus, due to gain in conformational entropy, unstable proteins ("soft" proteins; *e.g.* bovine serum albumin, beta-casein and catalase) generally adsorb on all surfaces independent of electrostatic interactions (25). In this process they tend to unfold and spread on the surface with time (25; 75; 76), this effect being faster on more hydrophobic surfaces (77). For stable ("hard" proteins), *e.g.* alpha-chymotrypsin and lysozyme, on the other hand, adsorption may occur readily on hydrophobic surfaces (with spreading (77)) but is weak on hydrophilic surfaces, unless there are favorable electrostatic interactions (25; 77).

Usually protein adsorption is irreversible on an experimental time scale (25). Therefore, the apparent behavior according to a Langmuir adsorption isotherm, with an increase in surface density at increased incubation concentration, may be attributed to different orientations and different degrees of conformational changes of the proteins following adsorption (77; 78). If the protein shape is approximated as rectangular one would expect energetically favored adsorption, with the long axis along the surface, at low solution concentration. On the other hand, at high concentration and high surface coverage, an orientation with the long axis perpendicular to the surface would be entropically favored (78). Moreover, as the surface coverage increases there may be structural transitions from the first to the second orientation. There may also be changes in conformation and protein-protein

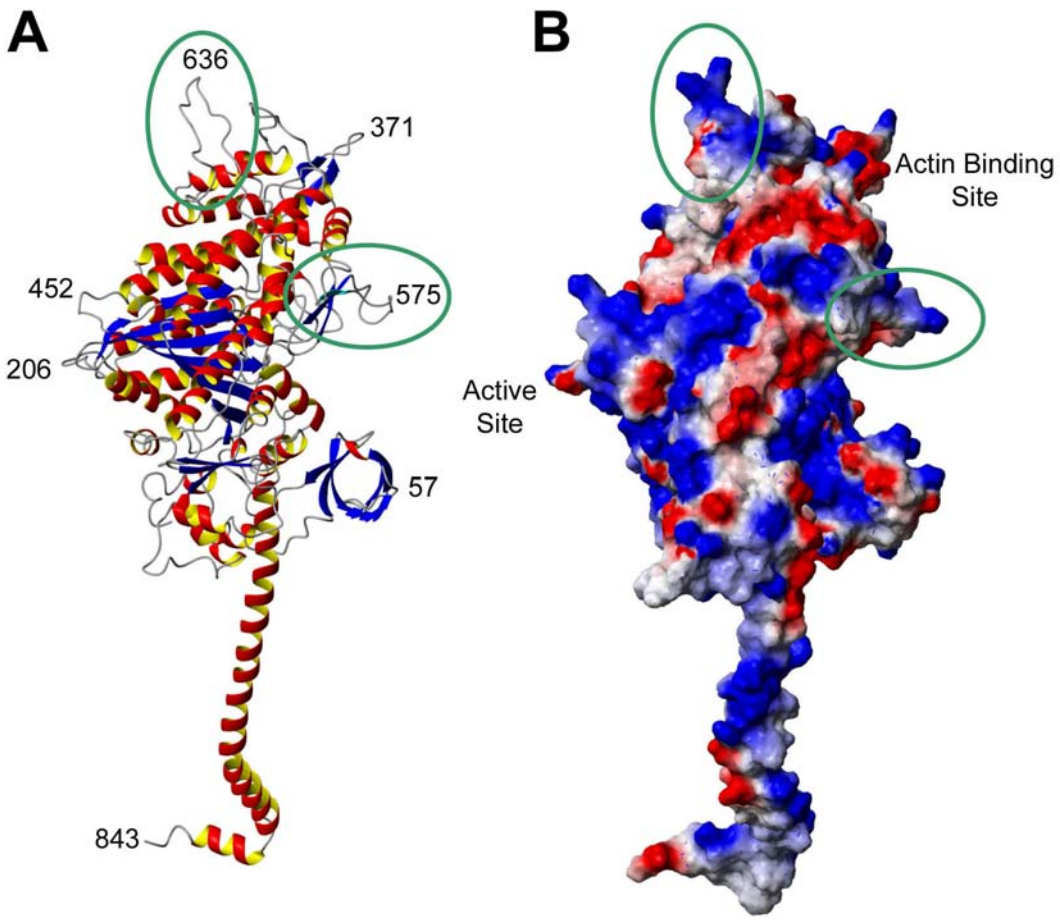


**Figure 5.** Model of the myosin heavy chain based on the crystal structure of myosin subfragment 1 (91). The myosin chain has four flexible loop segments, comprising residues 205-215, 572-574, 627-646 and 732-737, for which no, or very limited electron density could be detected by the X-ray analysis. To generate a model of the complete protein these four loops were built into the structure and their conformation energy minimized using the MacroModel package (Schrodinger). Panels A and B show the myosin head in a ribbon representation and in an electrostatic surface representation. Positive and negative charges are shown in blue and red, respectively. The Figure was prepared in Molmol (169) Highlighted in the model by green circles are the highly basic loops 567-575 (loop 3) and 626-647 (loop 2) which have been suggested to be crucial for effective actomyosin interactions (see text).

interactions (*e.g.* clustering and electrostatic attractions and repulsions (79; 80)) to increase or decrease the surface coverage. With regard to irreversible changes in conformation these more readily occur on hydrophobic surfaces and with "soft" proteins.

To summarize, at low surface coverage the important factors are the electrostatic and entropic interactions between the proteins and the surfaces. At high surface density these factors are complicated by different types of protein-protein interactions with the possibility of different protein orientations and conformations.

## 5. STUDIES OF MOTOR ADSORPTION TO SURFACES

### 5.1. Characterization of the motor

Studies of motor-surface interaction mechanisms focused on heavy meromyosin motor fragments from fast skeletal muscle will be described below. Relevant characteristics of the entire "long HMM fragment" (81) used in our studies and its major segments are described in Figure 5 and Table 3. Globally, the molecule is strongly negatively charged at physiological pH and both the entire HMM molecule and S1 are electric dipoles.

There is strong evidence, both from biochemical studies (82; 83) electron microscopy (84) and fluorescence microscopy (85) that the myosin hinge region, *i.e.* the C-terminal of long chymotryptic HMM (82), has properties that are characteristic of a "soft" protein that readily unfolds. On the other hand, the remaining subfragment 2 part of the HMM tail is likely to be more stable, exhibiting a "fine balance between coiled-coil propensity and structural instability" (86). The amino acid composition of the S2 part (as for the entire rod portion of myosin) is dominated by acidic amino acids with a large excess of

negative charge at physiological pH ( (82) and Swiss Prot-TrEMBL, entry name MYH4_RABIT).

This is in good agreement with a negatively charged backbone of the thick filament (87). Both this overall negative charge and the distribution of negatively charged residues on the S2 surface, may have important implications for regulation and modulation of muscle contraction (21; 86). The persistence length of S2 (88) is given in Table 3 in order to indicate the level of flexibility of this region, a factor that also may be of importance for the detailed orientation of the HMM molecules at a surface.

Since a part of the myosin heavy chain near the head-tail junction is susceptible to cleavage by papain one may expect some degree of flexibility with temporary unfolding in this region as discussed in (89; 90).

With regard to subfragment 1 the neck is stabilized by the essential and regulatory light chains (91) and it exhibits an overall negative charge, attributed to the light chains. On the basis of amino acid sequence, the algorithm of Guruprasad *et al.* (92), implemented in Swiss Prot-TrEMBL, classifies the catalytic domain of S1 as stable. Accordingly, it has been shown to exhibit a higher temperature of thermal unfolding than subfragment 2 (93). On the other hand, this temperature is lower than for the soft protein BSA (94). Moreover, the 50 kD segment of the catalytic domain has been shown to readily unfold *in vitro*, both in response to a prolonged but moderate increase in temperature (95) and in response to increasing concentrations of methanol (96).

Regarding charge distribution in the catalytic domain the accumulation of positively charged residues in the mobile surface loops 2 and 3 (Figure 5) is particularly notable. Both these mobile loops have been implicated in actin binding (2; 53) and electrostatic interactions have been shown to be important in stabilizing the actomyosin interactions in different nucleotide states. Since the loops may have the capability to protrude some distance above the S1 surface (68) they would be expected to give rise to electrostatic potentials that extend quite far into the solution.

Several detailed mutagenesis studies have been performed with loop 2 (2; 70; 97; 98). As reviewed by Geeves *et al.* (2), the number of positively charged amino acids in this loop is important for several aspects of the interaction between actin and myosin II. This includes the formation of the initial non-specific weak binding state, the actomyosin affinity in different nucleotide states, the actomyosin ATPase, and the degree of myosin based regulation of contraction. More recently, it has also been demonstrated that the positive charges in loop 2 are important for the affinity of the weakly actin binding state of myosin V (98). Moreover, the processive run length of myosin V was found to be reduced as a result of a decreased number of positive charges in loop 2, attributed to a reduced on-rate of the leading head (71). The above results suggest that positively charged residues in the mobile surface loops 2 and probably 3 (2; 68), are of great importance for guiding the diffusional search of the motor towards its binding site on actin. In addition to these charged loops the dipole characteristics of the entire S1 fragment is likely to be of importance in this connection. It also seems reasonable to presume that similar mechanisms are important in electrostatically driven surface adsorption of the motors at negatively charged surfaces.

### 5.2. Derivatization and characterization of the surfaces

In studies of motor-surface adsorption mechanisms, and in well-defined biophysical assays, adequately cleaned, functionalized and characterized surface substrates should ideally be used. A standardized and efficient cleaning procedure is important in order to produce well-defined surface chemistries for protein adsorption or further derivatization (*cf*. (8; 34; 99)). After physical-chemical characterization of the surfaces it is important to use them as soon as possible, at least within hours, to avoid environmental contamination (8; 99). Longer storage times are acceptable in a controlled environment*, e.g.* under pure distilled water (8), nitrogen atmosphere *etc.* (depending on the specific surface chemistry).

Simple surface derivatization may be achieved in different ways: *e.g.* by spreading of a nitrocellulose solution with subsequent evaporation of the solvent (13), spinning of polymers (100-102) and formation of covalent self-assembled monolayers on silicon-dioxide (8; 31; 34; 62; 103). The latter approach, using silane chemistry, is attractive since it is readily achieved on transparent glass or fused silica surfaces. Silane monolayers may also readily be nanostructured for selective localization of motility to nanosized tracks (104). However, for the purpose of reproducibility it is important to use monofunctional silanes, *e.g.* monochlorosilanes to avoid polymer formation (103).

In a recent study (8) several monochlorosilanes were tested as underlying substrates for the surface adsorption of HMM in motility assay studies. Here, it was shown that one of the simplest monolayers with trimethylsilyl residues on the surface (achieved by silanization using trimethylchlorosilane; TMCS) gave rise to the best and most reproducible function in motility assays. The motility was at least as good (in terms of velocity and fraction of motile filaments), and more reproducible, than on more poorly defined nitrocellulose surfaces (103; 105; 106).

As a prerequisite for understanding surface-protein interactions, a proper surface characterization is important. In earlier studies (8; 34; 103) silane monolayers and other surfaces have been characterized by contact angle measurements (probing surface hydrophobicity; Table 2), zeta-potential measurements (probing surface charge) and atomic force microscopy (probing surface topography and roughness). These characterization methods give a considerable amount of information but, if there is uncertainty about the chemical composition or film thickness, they may need to be supplemented by X-ray photoelectron spectroscopy (XPS; probing elemental

**Table 2.** Various experimental techniques for studies of surfaces and surface-protein interactions[1]

| Experimental technique | Principle | Information derived | Refs[3] | S/P [4] |
|---|---|---|---|---|
| **Ultrastructural/Scanning probe techniques** | | | | |
| Atomic force microscopy | A fine tip on a cantilever is scanned over a surface. The interaction forces (related to tip-surface distance) are utilized to image topography with sub-nm resolution. Also force-spectroscopy studies of elasticity and recognition | Surface topography, *e.g.* surface roughness. Imaging with tapping mode in fluid can give detailed images of proteins in their native state. Information about surface elasticity. | (108; 110; 141; 142) | S, P |
| Electron microscopy | Following, pre-treatment of the sample (necessary for biological specimens) a primary beam of electrons interacts with the specimen in vacuum to form an image | Studies of surface morphology usually with slightly better resolution than with AFM but with more severe requirements for pre-treatment of biological samples | (79; 84; 107; 143) | S, P |
| **Biochemical techniques** | | | | |
| ATPase and depletion of incubation solution, | See text | Catalytic activity and surface density of ATPase | (32; 34; 116) | P |
| Limited proteolysis of adsorbed proteins | See text | Information about immobilized and free parts of proteins | (119) | P |
| **Thermodynamic technique** | | | | |
| Contact angle measurements: advancing and receding angles. | Contact angle at triple point between gas phase, surface and small droplets. Advancing (receding) angle measured as droplet volume is slowly increased (decreased). | Surface hydrophobicity. Surface tension. Difference between receding and advancing angle: surface homogeneity. | (99; 144; 145) | S, (P) |
| **Spectroscopic techniques** | | | | |
| X-ray photoelectronspectroscopy (XPS) | Based on photoelectric effect. Bombardment with X-rays causes release of electrons from inner shells with kinetic energies characteristic of the molecular species | Detailed chemical composition and monolayer thickness | (143; 146) | S |
| Fourier transform infrared spectroscopy (FTIR) | Infrared spectroscopy exciting stretching and bending modes of chemical bonds. Fourier transform spectroscopy utilizes a interferometer to make data collection more effective | Structure and composition of thin surface films, *e.g.* self-assembled monolayers but also conformations of protein films e.g secondary structure information | (147) | S, P |
| Neutron reflectivity | Reflectivity of neutrons at solid-water interfaces | Layer thickness and identification of different layers and some aspects of chemical composition | (148) | S, P |
| Mass-spectroscopy *e.g.*TOF-SIMS[2] | Primary ion beam sputters particles from surface – ejected secondary electrons (1-1.5. nm from surface) are analyzed by time-of-flight mass spectrometry | Information about composition of the the top layer of a surface or protein film. This gives information about protein orientation | (74) | S, P |
| **Different optical techniques** | | | | |
| Ellipsometry | Altered state of polarized light upon reflection in different interfacial layers | Information about thickness and refractive index of surface coating. The latter parameter related to amount of protein | (122; 149) | S, P |
| FLIC-microscopy =fluorescence interference contrast microscopy | See text | Gives information about the distance between a given surface and a fluorescent probe | (6; 168) | (S), P |
| TIRF spectroscopy/ microscopy | See text | Protein density at surface but also some orientation information possible (*e.g.* by anisotropy studies) | (112; 123; 150) | (S), P |
| Surface Plasmon resonance (SPR) | Attenuation of reflected light due to resonance energy transfer to surface plasmons *e.g.* at a gold surface occurs at an angle that is sensitive to the refractive index, and thereby to the binding of proteins close to the surface | Binding of proteins to surface may be followed in real time by monitoring changes in refractive index close to the surface | (151; 152) | P |
| Optical waveguide lightmode spectroscopy (OWLS) | Grating assisted coupling of light into and guidance within an optical waveguide layer. Coupling to liquid cell makes the in-coupling angle sensitive to the refractive index of and adsorbed film. | By the derived information about refractive index and thickness of the protein film the amount of adsorbed protein can be calculated with high sensitivity. | (80; 153) | P |
| **Other methods** | | | | |
| Quartz crystal microbalance (QCM) | See text | Deposition of wet mass on surface and flexibility of protein film | (128; 131; 154, 155) | P |
| ζ-potential measurements | Measures potential (ζ-potential) at Stern layer *e.g.* on basis of electroosmotic flow rate | ζ-potential proportional to surface charge density. Depends on pH, ionic strength and exact ionic composition | (156) | S, (P) |

[1] General techniques for protein adsorption studies with potential usefulness for the study of surface-motor interactions are included. In addition to the cited papers some of which are rather specialized, overviews of several techniques are given in recent general reviews such as (10; 25; 143), [2]TOF-SIMS: time of flight secondary ion mass spectrometry, [3] References are selected for pedagogical general descriptions of the techniques as well as for illustrating potential usefulness for the study of different aspects of surface adsorption of motors. [4] Used for studies of surfaces (S) and/or proteins (P)

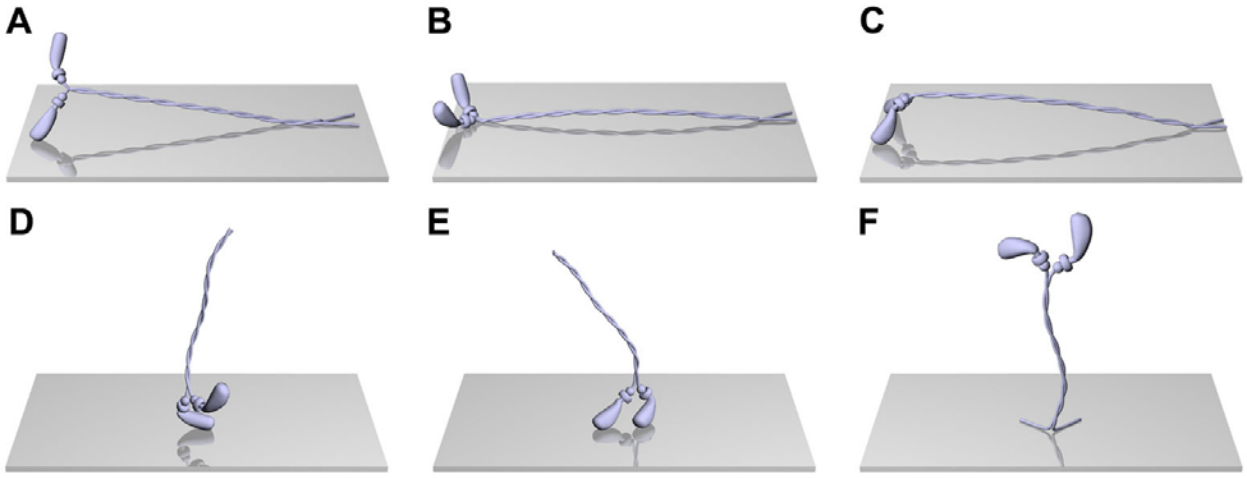


**Figure 6.** Schematic illustrations of the most likely configurations of surface adsorbed HMM molecules. Configurations selected on basis of experimental results and theoretical arguments (see text)

**Table 3.** Relevant properties of HMM and its segments

| HMM fragment | Length[1] | net charges[2] | dipole moment[3] | persistence length[4] |
|---|---|---|---|---|
| HMM[5] | 92 – 95 nm | -30 | 1800 D, at > 0.3. M ionic strength | ----- |
| S2 (AS 841 – 1361)[6] | 72 – 75 nm | -37 | | 130 nm |
| S2 (hinge region; AS ~1210-1360) | | | | ----- |
| S1 (AS 1-841; including light chains; RLC+ELC) | 20 nm | -9 | 1000 – 8000 D depending on ionic strength | ----- |
| S1 (head; AS 1-783) | | +2 | | ----- |

[1] Length of S2 according to (84; 124) and of rabbit S1 in buffer solution according to (166). [2] Charges calculated from sequence MYH4_RABIT using Swiss Prot-TrEMBL (Prot Param tool) assuming that glutamic acid and aspartic acid on one hand, and asparagine and lysine on the other, carry one negative and one positive elementary charge, respectively at pH 7.4. [3] Dipole moment of HMM and S1 from (124) and (167), respectively. [4] Persistence length of S2 from (88) assuming that it is equal to that for myosin rod. [5] With the conditions used in the referenced studies (*e.g.* (8; 34; 112)) HMM was prepared under conditions suitable for production of "long HMM molecules" (81). [6] Sequence corresponding to length of S2 according to (82) and comparison with entry MYH4_RABIT in Swiss Prot-TrEMBL. However, sequencing by Chen Lu (82) suggested considerably larger number of negatively charged amino acids in S2 than in sequence MYH4_RABIT. All other sequences from MYH4_RABIT.

composition and monolayer quality), infrared spectroscopy (probing molecular structure) or ellipsometry (probing layer thickness). These techniques, together with a number of other useful methods, are summarized in Table 2.

### 5.3. Characterization of surface-immobilized motors

There are a range of experimental techniques that can be implemented for characterization of proteins at surfaces and some of these are identical to those considered above for characterization of the surfaces themselves (Table 2). Below, we give a more detailed account of selected experimental techniques that, until now, have been used in studies of motor-surface interactions.

#### 5.3.1. Ultrastructural studies at low HMM coverage

Electron microscopy (EM; *e.g.* (84; 89; 107)) and, to a lesser extent, atomic force microscopy (AFM; (108; 109)), have been used to image individual surface-adsorbed molecules of myosin or, more seldom, HMM. However, these studies have not focused on surface-protein interactions and the surfaces have been characterized only to a limited extent. Moreover, the molecules are often dissolved in highly non-physiological solutions during deposition onto the surface (108).

The AFM and EM images have generally been obtained at motor densities too low for *in vitro* motility assays but suitable for single molecule studies. They often appear to show HMM or myosin molecules with their subfragment 2 part tethered to the surface along its length ( (84; 107); see discussion in (90)). Whether, one or both heads are free and extend above the surface is not always entirely clear (*cf.* (90)). Configurations, similar to those that may be seen in the ultrastructual images are schematically illustrated in Figure 6 A-C. In this representation, we have drawn the largest part of the subfragment 2 (S2) region above the surfaces (*e.g.* negatively charged mica or $SiO_2$), due to expected electrostatic repulsion (particularly at low ionic strength). It is also reasonable to presume that both heads of HMM are actually immobilized to negatively charged surfaces (such as mica and $SiO_2$) in several instances (Figure 6 C-E). Such immobilization of myosin V was for instance apparent in a fascinating movie compiled from AFM images obtained in high-speed scans ((110); http://www.s.kanazawa-u.ac.jp/phys/biophys/bmv_movie.htm). Whereas myosin V and myosin II have several structural differences, the motor domains are relatively well conserved. Accordingly, it has been presumed (2) that the basic mechanism of the docking mechanism with actin is similar *e.g.* involving electrostatic

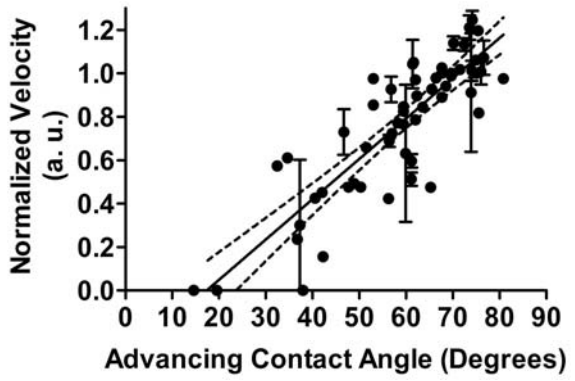


**Figure 7.** *In vitro* sliding velocity vs. advancing contact angle of the HMM adsorbing substrate. The latter constituted differently cleaned and silanized glass and silicon dioxide surfaces. The sliding velocity has been normalized to that on nitrocellulose surfaces tested on each given experimental occasion. Full straight line (obtained by linear regression) shown with 95 % confidence interval (dashed lines). Data, compiled and replotted from (8) and (34), obtained in assay solution with 0.6. % methylcelluose and an ionic strength of 130 mM.

interactions between positively charged surface loops on myosin and negatively charged regions on actin (see further above). It seems likely that the positively charged loops also are important in mediating adsorption of both myosin II and myosin V heads to negatively charged surfaces. Moreover, the initial adsorption in this region may be followed by partial unfolding of, *e.g.* the 50 kD segment. Thus, as outlined above, this region exhibits some characteristics of a "soft" protein component with potential for entropically driven adsorption.

An interesting feature in EM and AFM images is that myosin molecules seldom appear to cross each other in the images (*cf.* (32; 84; 109)). This is particularly striking in Figure 5a of Harada *et al.* (32) where very few crossings can be observed between neighboring molecules in spite of a rather high surface coverage. It is possible that this finding may reflect repulsion between the tail parts of different molecules as expected from their predominately negative charge. Interesting information from some EM-studies is the unwinding of the coiled-coil tail, corresponding to the LMM-HMM hinge region (84) which is also the target of chymotryptic cleavage in the preparation of HMM. Initial hydrophobic interactions between the hinge region and the surface, followed by subsequent further unfolding, seems to be a likely mechanism for entropically driven surface adsorption on both hydrophobic and hydrophilic surfaces (*cf.* above).

In the case of *in vitro* motility assay experiments the HMM density may vary between very low (requiring methylcellulose in the assay solution) and near saturating densities of 3000 – 6000 per square micrometer (see below). The latter densities are also used in most efforts to develop nanotechnological applications (*e.g.* (104; 111). Direct studies of HMM configurations (using EM and AFM), under these conditions, give limited information (*cf.* (32)). Instead more indirect methods have been used as outlined below.

**5.3.2. Studies of HMM adsorption at high surface coverage – effects of surface hydrophobicity and charge**

The mechanisms for HMM adsorption on hydrophilic and hydrophobic surfaces were studied in some detail in a series of recent studies (8; 34; 103; 112-114)) using a high (> 100 micrograms $ml^{-1}$) incubation concentration. The HMM-propelled actin filament sliding velocity decreased with a reduction in contact angle within the range 25 – 80 $^{o}$ for several silanized and non-silanized $SiO_2$ surfaces (Figure 7; (8; 34)). Here the decrease in contact angle was associated with increased negative charge of the surfaces (8). These results are in general agreement with a very recent study using glass, nitrocellulose and polymer surfaces with a range of contact angles between 30 and 80$^{o}$ (114). However, in the latter experiments there was a decrease in actin filament sliding velocity for contact angles above 70$^{o}$, possibly due to denaturation, caused by interaction of the proteins with the "soft" hydrophobic polymer surfaces. It is possible that the effect of contact angle on sliding velocity only occurs when changes in contact angle are associated with altered negative surface charge density since high quality motility was observed on positively charged polyelectrolyte surfaces (113).

Our studies of motility on different surface substrates have been accompanied by more detailed studies using model hydrophilic ($SiO_2$ and glass) and hydrophobic (TMCS derivatized $SiO_2$/glass) surfaces with contact angles < 30 $^{o}$ and > 70$^{o}$, respectively. These investigations are described in greater detail below, in parallel with an overview of the employed experimental techniques.

**5.3.2.1. Biochemical techniques**

Various biochemical methods have been applied for the quantification of motor density on surfaces and to obtain information about the mode of surface adsorption.

Different ATPase assays, *e.g.* based on the myosin K/EDTA ATPase (34; 115) or $NH_4$/EDTA ATPase (116), are the most frequently used methods for estimation of myosin surface densities. These methods are complicated by the rather high $K_M$ (0.3. – 0.4. mM) for both the myosin K/EDTA (117; 118) and $NH_4$/EDTA ATPase (118). Moreover, they rely on the assumption that the ATPase activity of surface-adsorbed motors is similar to that of motors in solution, an assumption that is not necessarily correct. Thus, a significant fraction of the surface adsorbed motors may be catalytically inactive (119) or, alternatively, the ATP turnover by surface adsorbed motors may be lower or, indeed also higher ((112); see further below), than by motors in solution. A convenient way to obtain the total amount of adsorbed protein is to measure the degree of depletion of the incubation solution using a sensitive protein concentration assay (referred to as depletion studies below; (32; 34)). Using this method the HMM density at near saturation (incubation with HMM at 120 micrograms $ml^{-1}$) was determined to 5400 ± 400 HMM

molecules per square micrometer (mean ± SEM, n = 5) on a TMCS surface (112) and slightly (~25 %) higher on $SiO_2$ (34). Previously (34), the use of a K/EDTA ATPase assay suggested a HMM density under similar incubation conditions of 6700 ± 380 per square micrometer (n = 2) on TMCS, 5800 ± 310 per square micrometer (n = 2) on nitrocellulose and about 5400 on $SiO_2$. These values were obtained on the assumption that the ATPase activity was similar to that in solution. However, taken together with the HMM depletion data, the results suggest that the average catalytic activity of HMM is higher after adsorption to TMCS than in solution. A similar result was recently (112) obtained for the steady-state MgATPase activity, based on analysis of ATP/Alexa-ATP and ADP/Alexa-ADP by HPLC, different times after the onset of multi-turnover hydrolysis.

Some variability between labs in HMM density has been observed for apparently similar incubation conditions. Thus, using nitrocellulose surfaces for HMM adsorption, Guo and Guilford (120) observed, on basis of $NH_4$/EDTA ATPase data, a HMM density of 3200 per square micrometer at nearly saturating conditions (incubation concentrations > 80 micrograms $ml^{-1}$). For myosin, K/EDTA ATPase measurements suggested a density at saturation of about 2000 per square micrometer on nitrocellulose (121) whereas depletion studies (32) gave a myosin density of about 4000 per square micrometer on siliconized surfaces. The above values should be compared to a theoretical maximum of slightly less than 12 000 per square micrometer based on optimal packing of the myosin heads (34).

Whereas the described methods measure the total surface density of motors, or the density of catalytically active motors (or indeed the catalytic activity), these quantities are not necessarily related in any simple way to the number of motors that are available to propel actin. This was clearly demonstrated in a recent study of heavy meromyosin motors adsorbed to $SiO_2$ surfaces. These motors had considerably poorer actin propelling capabilities than on a TMCS surface, in spite of a higher total motor density and only a slightly lower catalytic activity (see above). Indeed, there are rather limited possibilities to assess the actual density of motors with actin propelling capability. However, some relevant information may be derived from studies of actin binding in the absence of ATP and of sliding velocity *vs* length of the actin filaments (34). Whereas the relationship between the maximum number of bound actin filaments in the absence of ATP and HMM surface density may be complicated (different filament lengths, crowding effects *etc*.) it is clear that this relationship gives semi-quantitative information about the number of HMM molecules with actin binding capability. This was suggested by recent actin binding studies using TIRF spectroscopy (34) and QCM (8), where the degree of actin binding correlated better with the sliding velocity than with the total HMM density on the surfaces (see further below).

Another way to estimate the density of actin propelling myosin heads is by studying sliding velocity *vs* filament length (34; 115). Using this method we (34) observed a density of actin propelling myosin heads on a hydrophilic $SiO_2$ surface that was < 40 % of that on TMCS. This should be compared to the rather small differences in HMM density and catalytic activity on the two surfaces (see above).

The estimation of the number of actin propelling myosin heads from plots of velocity *vs* filament length requires a reliable estimate of the duty ratio, *i.e*. the fraction of the ATPase cycle time that a myosin head stays strongly attached to actin. Second, it is necessary to know the maximal distance from the actin filament at which a motor can be immobilized to the surface and still be available for force-producing interactions with actin. This distance is difficult to quantify exactly and it may be strongly affected by the mode of surface immobilization of the motors. This is indicated by experiments with immobilization of myosin via monoclonal antibodies directed towards the HMM-LMM hinge region (11). In these studies a lower surface density of HMM molecules (300 – 600 per square micrometer) was required to obtain the same sliding velocities for all filaments of lengths > 1 micrometer than in cases where HMM is immobilized by non-specific adsorption (~2000 per square micrometer; (115)). If the duty ratio is not affected by the mode of surface immobilization the only possible interpretation of these results seems to be that the effective reach of an HMM molecule is higher in the case of antibody based immobilization.

Among the biochemical experiments that have provided interesting information on the mode of surface adsorption of HMM and S1 on nitrocellulose surfaces are the limited proteolysis studies of Toyoshima (119). Unfortunately these results have not been described in full experimental details and they deserve follow-up investigations. Briefly, Toyoshima applied papain and alpha-chymotrypsin at different concentrations to S1 or HMM motor fragments adsorbed to nitrocellulose. Based on SDS-PAGE analysis of the immobilized and released proteolysis products Toyoshima suggested different modes of HMM and S1 immobilization on nitrocellulose surfaces. The HMM configurations suggested by Toyoshima are similar to those illustrated schematically in Figs. 6 B, D-F, with a configuration corresponding to that in Figure 6 F, being the one mainly responsible for propelling actin filaments.

#### 5.3.2.2. Fluorescence spectroscopy

Total internal reflection fluorescence (TIRF) spectroscopy is a useful tool for the study of surface immobilized proteins (122; 123). In contrast to transmitted light spectroscopy it enables selective excitation of only those fluorophores that are located in the close proximity (~ 100 nm) of a solid surface. TIRF relies on the formation of an evanescent electromagnetic wave that arises at the interface between two transparent media (*e.g.* quartz and water, Figure 8A) when an incident beam of light is totally reflected (123). In brief, when a beam of light propagating within a transparent medium of high refractive index ($n_1$) (*e.g.* quartz) encounters a planar interface with a medium of

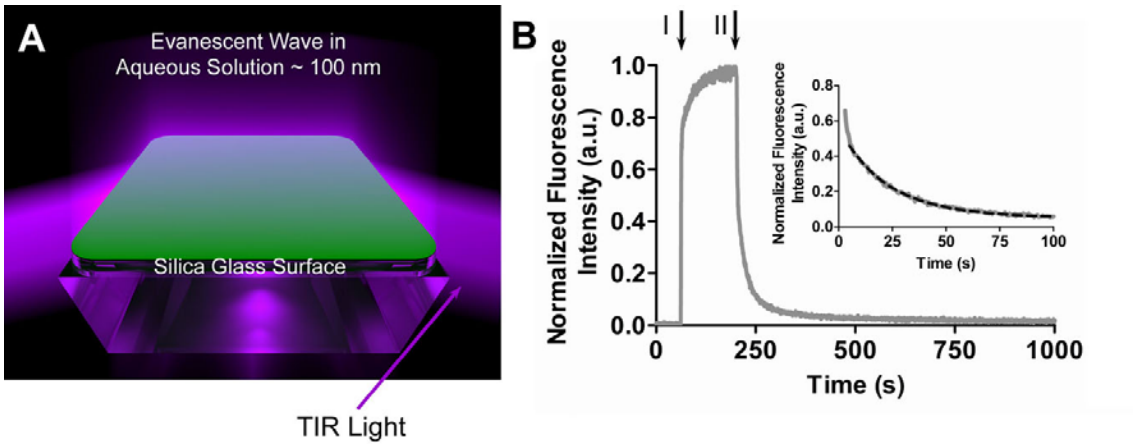


**Figure 8.** Total internal reflection fluorescence (TIRF) spectroscopy. (A) Schematic illustration of TIRF setup showing the quartz prism with a TMCS derivatized fused silica surface. Also indicated in the image is totally internally reflected (TIR) light beam and the resulting evanescent wave (fading blue/violet colour above slide surface). (B) Fluorescence intensity plotted against time for TIRF flow cells (TMCS surface) incubated with 3 micromolar Alexa-ATP following pre-incubation with HMM at 120 micrograms $ml^{-1}$. Data normalized to peak value of the fluorescence signal. Alexa-ATP incubation at first arrow (I). Following complete binding of the Alexa-ATP to HMM, the flow cell was quickly flushed (at second arrow:II) with Alexa-ATP free, but ATP containing, solution. Inset shows the first 100 s of the decaying fluorescence signal caused by turnover and release of Alexa-ATP from the HMM active sites. Triple-exponential functions fitted by non-linear regression shown as dashed black line ($y = 0.48e^{-0.048t} + 0.067e^{-0.0065t} + 0.020^{-0.00028t}$ and $r^2 = 0.993$). T = 25°C ± 0.5.°C. The amplitudes of the exponential processes sum up to 0.56.The difference from 1 is attributed to bulk contributions (*cf.* (112)). Small excitation slit used, making effects of photobleaching negligible, as suggested by studies where the slit width and total excitation time were varied.

lower refractive index ($n_2$) (*e.g.* water) the light undergoes TIR, under the condition that the angle of incidence is greater than a certain critical angle. The sine of this angle is given by the ratio $n_2/n_1$ (123).

When the criteria for TIR are met the main part of the incident radiation energy is reflected back into the high-refractive index medium. However, energy that penetrates through the interface gives rise to the "evanescent electromagnetic wave". The intensity of this wave decays exponentially with perpendicular distance from the interface, with a length constant, the penetration depth, on the order of 100 nm. The exact magnitude of the penetration depth is proportional to the wavelength of the incident light and is also a function of the angle of incidence and the refractive indices, $n_1$ and $n_2$ (123).

The HMM adsorption mechanisms on hydrophobic (TMCS) and hydrophilic (pure $SiO_2$) surfaces were investigated using TIRF spectroscopy (34; 112). In these studies Sundberg *et al.* (34) found, in agreement with depletion studies (see above), that the degree of HMM adsorption was slightly higher on $SiO_2$ (with poor motility) than on TMCS (with high quality motility). As briefly mentioned above, additional TIRF studies showed that the actin binding capability of TMCS-adsorbed HMM was several-fold higher than for the HMM molecules on $SiO_2$.

When using TIRF spectroscopy for protein adsorption studies, it is important to take into account the fact that proteins adsorbed in a configuration with their fluorescent groups in close proximity to the surface will be subjected to a higher evanescent wave intensity. Solely for this reason one would expect a higher fluorescence intensity than for other fluorescent groups located further away from the surface. For most proteins, these effects would be of minor importance. However, for HMM, with a length, up to about 90 nm (*e.g.* (124), the situation may be different. Interestingly, in this connection, we found that the average fluorescence intensity of a fluorescent ATP analogue at the active site of HMM was more than two times larger on $SiO_2$ than on TMCS (submitted manuscript). Although there are different possibilities to account for this finding, it is in accordance with the idea that the myosin heads, on average, are markedly closer to the surface on $SiO_2$ than on TMCS. This is also consistent with the motility assay results and actin binding studies showing poor function for HMM molecules on $SiO_2$.

The myosin ATPase activity of surface-adsorbed HMM molecules can also be assessed using TIRF spectroscopy and a suitable fluorescent ATP analogue (112). We recently (112) characterized, and used, the analogue adenosine 5'-triphosphate Alexa Fluor® 647 2'-(or 3')-O- (N- (2-aminoethyl) urethane), hexa (triethylammonium) salt (Alexa-ATP) for this purpose. The TIRF flow cell, with a TMCS derivatized fused silica surface (Figure 8A), was first incubated with HMM (Figure 3) followed by fluorescent Alexa-ATP at micromolar concentration (first arrow in Figure 8B). Upon complete binding of Alexa-ATP to the active sites of the surface-adsorbed motors, single turnover of the fluorescent analogue was initiated by quickly exchanging the bulk solution (second arrow in Figure 8B) for a buffer where Alexa-ATP had been exchanged for regular ATP. The Alexa-ATP turnover rate was then calculated by fitting the data to a triple exponential decay function (inset in Figure 8B). This yielded one dominating fast process that

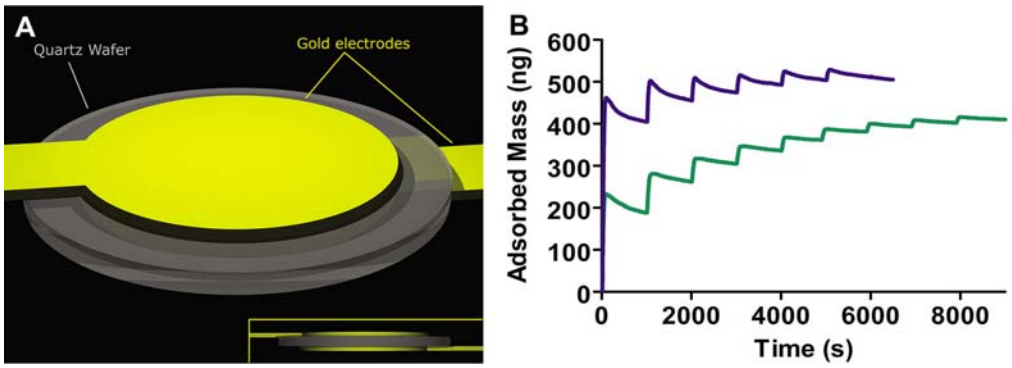


**Figure 9.** (A) The QCM consists mainly of a thin quartz crystal in between two gold electrodes (yellow). The proteins are deposited onto one of these electrodes possibly sandwiched via a $SiO_2$ layer. Inset in lower right corner illustrates side-view of sensor element. (B) Typical differences between TMCS and $SiO_2$ surfaces in the mass change recorded by a QCM sensor, upon repeated injections of HMM. TMCS: green line. $SiO_2$: blue line. At time, 0 s the signals are at 0 ng. Each injection of HMM (120 micrograms $ml^{-1}$), 12 flow cell volumes during 80 s, leads to a vertical shift in the signal. Absolute mass changes were calculated according to the Sauerbrey equation. Data re-plotted from ref (8).

constituted approximately 80 % of the total signal and exhibited a rate similar to that for turnover of Alexa-ATP in solution. Moreover, there were two processes that were significantly slower. One obvious interpretation of these data is that there are at least three different HMM configurations on the TMCS surface. One of these with approximately the same turnover rate as for HMM in solution and two with significantly reduced ATPase activity. It is reasonable to presume that the latter configurations have their heads tethered to the surface since immobilization of myosin heads, whether by surface adsorption (125; 126) or other mechanisms (126), have been associated with reduced ATP turnover rate. However, although the fraction of the myosin heads on $SiO_2$ that exhibited a low rate of Alexa-ATP turnover was larger than on TMCS, it was still small considering the very marked reduction of actin binding and actin propelling capability on this surface (submitted manuscript). This suggests that there are several HMM molecules on $SiO_2$ that have an ATPase activity similar to that in solution but nevertheless have their heads close to the surface, thus being inaccessible for actin binding. Possibly, these may be more weakly tethered to the surface (*e.g.* configurations in Figure 6 A-B and D) than the heads that exhibit reduced turnover rate (*e.g.* configurations in Figure 6. C and E).

#### 5.3.2.3. Microscopy

Various types of microscopy are useful for studies of motor-surface interactions. The use of TIRF microscopy would enable similar types of studies, as described above for TIRF spectroscopy, but with considerably more detailed information regarding spatial differences over a surface. Whereas there are several other microscopy techniques that may be useful for studies of surface adsorbed proteins fluorescence interference contrast (FLIC) microscopy is of particular interest. This technique was used recently (6) to characterize the distance above the surface at which microtubules are propelled by surface-adsorbed kinesin molecules. Here, use is made of the interference between various light paths on reflecting surfaces. Thus, the excitation light can either excite the fluorophores of the studied object (*e.g.* fluorescently labeled filaments) directly, or via reflection in an underlying $Si/SiO_2$ interface. Moreover, the emitted light reaches the detector either directly, or via the reflected path. The resulting interference between the direct and reflected light gives rise to modulation of the intensity of a fluorescent object as function of its distance from the reflective interface. By varying the thickness of the underlying $SiO_2$ surface this enables an accurate estimate of the distance from the fluorescent filament to the surface.

#### 5.3.2.4. QCM

Quartz crystal microbalance (QCM; Figure 9A) is a technique for mass sensing (127; 128) that, in the last decade, has experienced a rapid growth of new applications in biology and bio-interface science (129). The basis for the QCM technique is the piezoelectric properties of the quartz crystal with the generation of a mechanical response in synchrony with application of an alternating voltage. Usually, in QCM applications, an oscillating electric field is applied to the quartz crystal at its fundamental frequency, and subsequent changes in the resonance frequency are recorded as mass is deposited on the crystal. In 1959, Sauerbrey (130) showed that, in air, the changes in frequency, for a thin, rigid and homogeneous film of deposited material is directly proportional to the deposited mass.

In a liquid, and with viscoelastic surface films in general, the change in frequency is not directly proportional to the deposited mass and the Sauerbrey equation does not hold. This is attributed to a viscous, dissipative component causing the oscillation of the film to not fully couple into the oscillation of the crystal. Moreover, the frequency change is affected by the mass contributed by water molecules that are coupled to the surface-immobilized biomolecules of interest. This will cause the mass to be higher than that which can be attributed to the adsorbed proteins themselves (131). For this reason, QCM data will give a higher mass of adsorbed proteins, than the dry

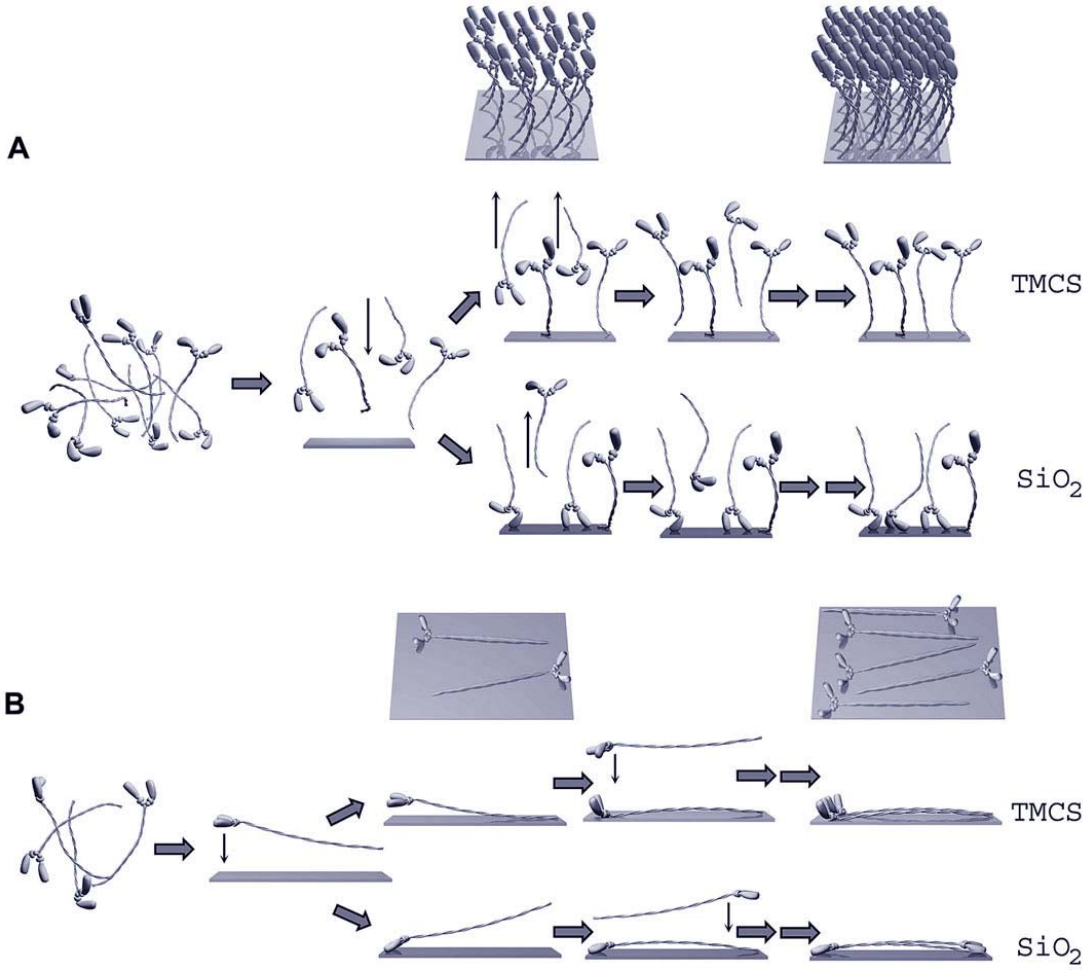


**Figure 10.** Model for adsorption of HMM to $SiO_2$ (low contact angle and high negative charge density) and TMCS derivatized $SiO_2$ surfaces (high contact angle and low charge density). (A) Different steps in the adsorption process for TMCS (upper row) and $SiO_2$ (lower row) are illustrated. First (left), the HMM molecules diffuse towards the surface where they are assumed to be partly ordered leading to adsorption with their long axis perpendicularly to the surface. This is described in detail in the text, together with the postulated subsequent events in the adsorption process. This process is expected to result in an almost complete HMM monolayer (upper panel in A; right). (B) The adsorption process at low HMM concentration in the incubation solution leading to adsorption of the HMM molecules with their entire length along the surface (see text for details).

protein mass obtained on basis of ellipsometry (131) or depletion studies.

It is possible to calculate the effective layer thickness, if both the hydrated mass (measured with QCM) and the dehydrated protein mass (*e.g.* through depletion studies or ellipsometry) are known (131). Such calculations were performed on basis of experimental studies for TMCS and $SiO_2$ surfaces (8). The results showed an apparent HMM-water film thickness of 30-40 nm for $SiO_2$, after one injection of HMM at 120 μg $ml^{-1}$, compared to 10-20 nm for TMCS. The effect on the recorded mass (according to the Sauerbrey equation), of several consecutive injections with HMM, are illustrated in Figure 9B. In accordance with the TIRF results in Figure 3 it is clear that, for each injection, HMM is adsorbed, followed by desorption in the interval between the injections. It is also clear that the rate of this desorption is reduced with subsequent incubations, suggesting slow conformational changes of HMM on the surface. It can also be seen that the total adsorbed mass, after one injection, is about 2 times higher on $SiO_2$ than on TMCS. This should be compared to only 25 – 30 % higher HMM density (34) for similar incubation conditions in both depletion and TIRF studies. In view of the latter results, the marked difference in mass and the related large difference in layer thickness on TMCS and $SiO_2$ can be taken as strong evidence for markedly different HMM configurations on the two surfaces (8). Due to the effect of dissipation, mentioned above, the total thickness of an adsorbed layer is always underestimated in liquid (131). Thus the estimated thickness of 30-40 nm for the HMM layer on $SiO_2$, suggests that a large fraction of the HMM molecules extend by almost their entire length, perpendicularly above the surface. Detailed interpretation

of the layer thicknesses and the amounts of adsorbed mass according to the Sauerbrey equation, will require further studies, *e.g.* including estimates of the degree of energy dissipation (131) on the different layers. Without such information, it cannot be excluded that the apparently lower thickness of the HMM layer on TMCS (compared to that on $SiO_2$) is due to a larger flexibility of the layer, rather than to a lower actual thickness. The idea of a larger flexibility would be in better agreement with theoretical considerations (8) and TIRF-measurements (see above) suggesting that the myosin heads are far away from the TMCS surface with the HMM molecule extending almost perpendicularly from the surface.

**5.4. Model for HMM adsorption on negatively charged hydrophobic and hydrophilic surfaces**

Taken together, the studies described above, suggest that there are only minor differences in HMM density between hydrophobic and hydrophilic surfaces at standard high incubation concentrations (> 100 micrograms $ml^{-1}$). Instead the differences in motility between the different surfaces are attributed to different HMM configurations. Thus, HMM molecules, with the heads unavailable for actin binding (*e.g.* tethered to the surfaces as the configurations in Figure 6A, C-E), appear to dominate on negatively charged hydrophilic surfaces. This is consistent with low actin binding detected using TIRF-spectroscopy and QCM and the poor motility with marked dependence of sliding velocity on actin filament length. The results are also consistent with ATPase studies and TIRF-spectroscopy records for the HMM-binding and turnover of Alexa-ATP. In contrast to the situation for the negatively charged hydrophilic surface, HMM molecules that readily bind actin filaments dominate on hydrophobic surfaces such as TMCS (*e.g.* configuration in Figure 6F).

Based on these results, and the properties of the HMM molecules and the surfaces, a model has been proposed for HMM adsorption to TMCS and $SiO_2$ (see further (8; 34; 112). This model is illustrated in Figure 10 for both high and low HMM density. It is reasonable to presume that the HMM molecules approach the surface from bulk solution in different orientations depending on the incubation concentration. This may be attributed to orienting effects on the HMM and S1 dipoles close to charged surfaces and electrostatic repulsion between S2 fragments of neighboring molecules. For high HMM incubation concentrations one would expect the course of events illustrated in Figure 10A. First, the HMM molecules are expected to approach the surface with either their head or hinge part with equal probability. However, if adsorption occurs only at the hinge region (on TMCS) the HMM molecules approaching via their head part will diffuse away allowing new molecules to enter the empty space, possibly in a favorable orientation. This process will be expected to continue until all available surface sites are occupied, ideally corresponding to about 12 000 HMM molecules per square micrometer (8). Under these conditions a vast majority of the heads would have the head up orientation. On $SiO_2$, adsorption may be considerably more likely with the head down configurations, as guided by electrostatic interactions possibly followed by a stronger entropically driven adsorption (25; 95; 96). Under these conditions a majority of the HMM molecules would end up with their heads adsorbed to the surface.

At low HMM incubation concentrations there are no orienting effects due to repulsion between neighboring HMM molecules. Therefore, it is reasonable to assume that a large fraction of the HMM molecules approach the surface with their long axis nearly parallel to the surface. Moreover, there is no steric hindrance or electrostatic repulsions due to other HMM molecules that would prevent two-site surface immobilization, *e.g.* at the LMM-HMM hinge on one hand, and the head-tail junction (*e.g.* on TMCS) or the actin binding site of S1 (*e.g.* on $SiO_2$), on the other. Thus, it is not unreasonable that such attachment occurs, although one of the attachment points may be weak allowing a reversible switch between different configurations.

Some of the experimental results that form the basis for the model in Figure 10 are subject to uncertainties as regards detailed interpretation (*cf.* QCM data above). However, the predictions of the model would be readily testable by further experiments. For instance, the importance of electrostatic interactions may be evaluated by adsorption experiments at different ionic strengths and using both positively and negatively charged surfaces. Likewise, the average distance of the myosin heads from different surfaces should be testable using FLIC-microscopy ( (6); see above), and QCM measurements that include evaluation of the energy dissipation ( (131); see above). If these and other experiments, *e.g.* using techniques in Table 2, will corroborate the model in Figure 10, it is clear that there are a number of important differences between the *in vitro* motility and single molecule assays and the *in vivo* situation. The precise nature of these differences may vary depending on the surface density of motors and they involve 1. a variable fraction of the myosin heads in inactive conformations/orientations with respect to actin propelling capacity and/or catalytic activity; 2. different orientations/conformations within the population of actin propelling heads, and 3. larger distance between the myosin heads and the underlying surface than in the thick filament in muscle. Finally, caution is needed when interpreting *in vitro* motility assays and optical tweezers studies using genetically engineered motors modified with respect to charged or hydrophobic residues. In addition to affecting actomyosin interactions, such manipulations could affect motility or force-generation by differences in surface-protein interactions.

It should be pointed out that the model was developed on basis of experimental results without BSA blocking and on basis of theoretical considerations, neglecting such blocking. This may have important effects at low HMM density and BSA-blocking may indeed be essential in such experiments to prevent domination of surface-motor interactions. In some experimental studies at low HMM surface densities, BSA has been present in all solutions subsequent to the first HMM incubation of the surface. Whereas this may be essential in order to prevent

the loss of BSA-blocking during the course of the experiment, there may also be unpredictable effects due to protein exchange at the surface causing reduced HMM density with time (132). At high HMM surface coverage, effects of BSA blocking appear to be negligible. First, using TIRF-spectroscopy (unpublished data) we failed to detect any significant BSA adsorption to a surface that was pre-incubated with HMM at 120 micrograms $ml^{-1}$ (for 2 min). Moreover, no effect on motility quality was observed (8) if the BSA blocking step was omitted. Indeed, these results are not surprising since the surface has been shown to be nearly saturated with HMM after one incubation step (120 micrograms $ml^{-1}$ for 2 min), and several hours of incubation was required to further increase the HMM density up to that of a theoretical monolayer (8; Figure 9).

As outlined above, effects of pH, ionic strength, specific ionic composition and temperature will affect not only the actomyosin interaction, but also surface-protein interactions. This may contribute to differences between *in vivo* experimental results and those obtained with *in vitro* motility assays or optical tweezers studies of single molecules.

## 6. PERSPECTIVES

### 6.1. Nanotechnological developments and basic studies of surface-protein interactions

A better understanding of surface- motor interactions is of high importance for nanotechnological and biotechnological applications of motors.

For instance, experimental results have clearly shown that the catalytic activity of HMM molecules may be high even on surfaces with markedly suppressed motility. This may be a disadvantage in lab-on-a-chip applications since these motor will contribute to the depletion of ATP and accumulation of ADP and $P_i$ (104). It may therefore be of interest to completely suppress adsorption of motors outside the motor propelling tracks, *e.g.* by using PEG-coated surfaces (133).

However, a dissociation between the motility quality and ATPase activity on a given surface may also be exploited, allowing further development of a heavily miniaturized high-throughput *in vitro* motility assay proposed recently (24; 104). This system encompassed circular closed loop TMCS tracks for motility, surrounded by, and encircling motility suppressing hydrophilic surfaces (total observed area ~10 square micrometers). Here, the myosin ATPase activity may be evaluated from turnover of fluorescent ATP molecules by the motors adsorbed on the hydrophilic areas whereas motility is evaluated from sliding on the TMCS tracks. Due to miniaturization this arrangement would allow parallel analysis of the simultaneous effects of thousands of different chemicals on sliding velocity and basal myosin ATPase activity.

More detailed knowledge of surface-motor interaction mechanisms will create the necessary foundations for engineering a robust motor-surface system for lab-on-a-chip applications. Such a system should be characterized by long-term, high quality motility by appropriate engineering of both surfaces and proteins to achieve correct motor orientation associated with minimal desorption and denaturation of the motors.

Under some experimental conditions HMM-induced actin filament sliding can be selectively localized to 50 - 100 nm wide TMCS tracks, with the exclusion of motility on the surrounding hydrophilic surfaces (104; 111) (*cf*. Figure 1) if these have a contact angle lower than about 60 $^{o}$ (34, 104). This suggests that HMM function reports surface properties corresponding to the macroscopic contact angle on areas of dimensions down to the HMM molecule size. Thus, actin sliding velocity on nano-sized lines may be useful for quantitative nanoscale characterization of surface chemistry related to the macroscopic contact angle (*cf*. (8)). Presently, atomic force microscopy (lateral force microscopy (134)) is the only technique available for similar purposes.

The dependence of sliding velocity on the contact angle and degree of negative charge of the surface suggests possibilities to reversibly, and locally, modulate actomyosin motility in nanotechnological applications (16), *e.g*. by light induced switching of surface hydrophobicity (135). However, this requires reversible rearrangements between the different HMM configurations without irreversible desorption of HMM. Whether this is indeed possible, remains to be shown.

The fact that HMM/myosin motors exhibit significant adsorption to both hydrophobic and hydrophilic surfaces is different from the behavior of several other proteins (136) that appear to predominately adsorb to hydrophobic surfaces. However, it is not unexpected in view of the diverse structural domains of the motor proteins (Figs. 5 - 6 and Table 3). Additionally, by only considering the myosin head (S1), this exhibits a rather unique "molecular surface" (17) that varies depending on the nucleotide species at the active site. For these reasons, it would be of interest to compare the adsorption behavior of myosin and its *proteolytic* fragments to that of other proteins, for which adsorption phenomena have been studied in greater detail. Finally, due to the multitude of different functionalities, myosin and HMM may be interesting test proteins for critical testing of non-fouling properties of protein repellant surfaces.

### 6.2. Biophysical assays

It seems clear from several of the results, reviewed above, that it is of uttermost importance to take surface-motor interactions into account in the interpretation of IVMA and optical tweezers experiments, and in the extrapolation of such results to the *in vivo* situation. Insights into motor-surface interactions may also contribute to the understanding of myosin based regulation in non-skeletal muscle myosin and modulation of contraction in skeletal muscle by phosphorylation of regulatory light chains. The binding of myosin heads to negatively charged surfaces may here be regarded as analogous to the association of the myosin heads to the negatively charged, thick myosin filaments in the relaxed state of muscle.

It would be of interest to produce ordered arrays of myosin motors *in vitro* to probe cooperative interactions that may require maintained ordering of the contractile proteins (24). Such cooperative interactions could occur between the two heads of each myosin II molecule as suggested by a number of studies (41; 137-139).

The studies of motor surface interactions suggest that ordered arrays of motors may be difficult to achieve based on non-specific adsorption of HMM, *e.g* combined with specific nanostructuring and electric field based orientation (24). At high HMM densities such ordering would be inefficient due to apparently flexible surface attachment of the motor. At low HMM densities the ordering may be possible in principle, provided that there are at least two interaction points per HMM molecule as suggested in Figure 6 A-C. However, also under these conditions there is always the risk that, at least one of the heads, is prevented to interact with actin, *e.g.* through strong interactions with the surface. This risk may be similar with specific attachment at certain points along the myosin molecule, *e.g.* by the introduction of complementary functionalities on the surfaces (using nanolithography) and on the motor (by protein engineering). A third possibility is attachment of motors to surfaces via monoclonal antibodies raised against specific regions of HMM. However, this method, found in a previous study to have some advantages (11), required more complex experimental procedures and does not solve possible problems related to efforts to achieve firm orientation of the motors. Moreover, the underlying antibody surface may, as well as the artificial surface, have properties different from the underlying myosin filament surface in the muscle.

Thus, on the basis of available evidence, thick filaments, and preferably native ones may be required as immobilization scaffolds for the motors in order to enable the *in vitro* demonstration of some *in vivo* phenomena. Such *in vivo* properties may involve the postulated cooperative interaction between the two heads of myosin II under some experimental conditions. In order to observe these properties *in vitro* it may also be necessary to study interactions of the ordered array of heads with two actin filaments cross-linked at a distance similar to that *in vivo* (107; 140)).

## 7. ACKNOWLEDGEMENTS

The work was supported by grants from The Swedish Research Council (Project # 621-2004-3449), The Carl Trygger Foundation, The Knowledge Foundation (KK-stiftelsen), The Crafoord Foundation and The Faculty of Natural Sciences and Engineering, University of Kalmar.

## 8. REFERENCES

1. J Howard: Mechanics of motor proteins and the cytoskeleton. Sinauer Associates Inc, Sunderland, MA, 1-367. (2001)

2. MA Geeves, R Fedorov, DJ Manstein: Molecular mechanism of actomyosin-based motility. *Cell Mol Life Sci* 62, 1462-77 (2005)

3. J Clemmens, H Hess, R Lipscomb, Y Hanein, KF Bohringer, CM Matzke, GD Bachand, BC Bunker, V Vogel: Mechanisms of microtubule guiding on microfabricated kinesin-coated surfaces: Chemical and topographic surface patterns. *Langmuir* 19, 10967-10974 (2003)

4. Y Hiratsuka, T Tada, K Oiwa, T Kanayama, TQ Uyeda: Controlling the direction of kinesin-driven microtubule movements along microlithographic tracks. *Biophys J* 81, 1555-61. (2001)

5. SG Moorjani, L Jia, TN Jackson, WO Hancock: Lithographically patterned channels spatially segregate kinesin motor activity and effectively guide microtubule movements. *Nano Letters* 3, 633-637 (2003)

6. J Kerssemakers, J Howard, H Hess, S Diez: The distance that kinesin-1 holds its cargo from the microtubule surface measured by fluorescence interference contrast microscopy. *Proc Natl Acad Sci U S A* 103, 15812-7 (2006)

7. T Fischer, H Hess: Materials chemistry challenges in the design of hybrid bionanodevices: supporting protein function within artificial environments. *Journal of Materials Chemistry* 17, 943-951 (2007)

8. N Albet-Torres, J O´Mahony, C Charlton, M Balaz, P Lisboa, T Aastrup, A Mansson, IA Nicholls: Mode of Heavy Meromyosin Adsorption and Motor Function Correlated with Surface Hydrophobicity and Charge. *Langmuir* 23*,* 11147 - 11156 (2007)

9. F Rusmini, ZY Zhong, J Feijen: Protein immobilization strategies for protein biochips. *Biomacromolecules* 8, 1775-1789 (2007)

10. B Kasemo: Biological surface science. *Surface Science* 500, 656-677 (2002)

11. DA Winkelmann, L Bourdieu, A Ott, F Kinose, A Libchaber: Flexibility of myosin attachment to surfaces influences F-actin motion. *Biophys J* 68, 2444-53 (1995)

12. A Ishijima, H Kojima, T Funatsu, M Tokunaga, H Higuchi, H Tanaka, T Yanagida: Simultaneous observation of individual ATPase and mechanical events by a single myosin molecule during interaction with actin. *Cell* 92, 161-71 (1998)

13. SJ Kron, YY Toyoshima, TQ Uyeda, JA Spudich: Assays for actin sliding movement over myosin-coated surfaces. *Methods Enzymol* 196, 399-416 (1991)

14. JT Finer, RM Simmons, JA Spudich: Single myosin molecule mechanics: piconewton forces and nanometre steps. *Nature* 368, 113-9 (1994)

15. H Hess, GD Bachand, V Vogel: Powering nanodevices with biomolecular motors. *Chemistry-a European Journal* 10, 2110-2116 (2004)

16. A Mansson, M Sundberg, R Bunk, M Balaz, IA Nicholls, P Omling, JO Tegenfeldt, S Tagerud, L Montelius: Actin-based molecular motors for cargo transportation in nanotechnology - Potentials and challenges. *IEEE Trans Adv Pack* 28, 547-555 (2005)

17. DJG Bakewell, DV Nicolau: Protein linear molecular motor-powered nanodevices. *Aust J Chem* 60, 314-332 (2007)

18. MGL van den Heuvel, C Dekker: Motor proteins at work for nanotechnology. *Science* 317, 333-336 (2007)

19. H Hess, J Clemmens, D Qin, J Howard, V Vogel: Light-controlled molecular shuttles made from motor proteins carrying cargo on engineered surfaces. *Nano Letters* 1, 235-239 (2001)
20. L Ionov, M Stamm, S Diez: Reversible switching of microtubule motility using thermoresponsive polymer surfaces. *Nano Letters* 6, 1982-1987 (2006)
21. RJC Levine, ZH Yang, ND Epstein, L Fananapazir, JT Stull, HL Sweeney: Structural and functional responses of mammalian thick filaments to alterations in myosin regulatory light chains. *J Struct Biol* 122, 149-161 (1998)
22. DM Warshaw, JM Desrosiers, SS Work, KM Trybus: Smooth muscle myosin cross-bridge interactions modulate actin filament sliding velocity *in vitro*. *J Cell Biol* 111, 453-63. (1990)
23. JJ Gray: The interaction of proteins with solid surfaces. *Curr Opin Struct Biol* 14, 110-5 (2004)
24. A Mansson, IA Nicholls, P Omling, S Tagerud, L Montelius: Nanotechnology enhanced functional assays of actomyosin motility - potentials and challenges. In: Controlled nanoscale motion, Lecture Notes in Physics 711. Eds: Linke H, Mansson A, Springer, Berlin Heidelberg. Germany, 385-406 (2007)
25. K Nakanishi, T Sakiyama, K Imamura: On the adsorption of proteins on solid surfaces, a common but very complicated phenomenon. *J Biosci Bioeng* 91, 233-244 (2001)
26. V Hlady, J Buijs: Protein adsorption on solid surfaces. *Current Opin Biotechnol* 7, 72-77 (1996)
27. MP Sheetz, JA Spudich: Movement of myosin-coated structures on actin cables. *Cell Motil* 3, 485-9 (1983)
28. JA Spudich, SJ Kron, MP Sheetz: Movement of myosin-coated beads on oriented filaments reconstituted from purified actin. *Nature* 315, 584-6 (1985)
29. SJ Kron, JA Spudich: Fluorescent Actin-Filaments Move on Myosin Fixed to a Glass-Surface. *Proc Natl Acad Sci U S A* 83, 6272-6276 (1986)
30. JR Sellers, G Cuda, F Wang, E Homsher: Myosin-specific adaptations of the motility assay. *Methods Cell Biol* 39, 23-49 (1993)
31. HM Warrick, RM Simmons, JT Finer, TQ Uyeda, S Chu, JA Spudich: *In vitro* methods for measuring force and velocity of the actin-myosin interaction using purified proteins. *Methods Cell Biol* 39, 1-21 (1993)
32. Y Harada, K Sakurada, T Aoki, DD Thomas, T Yanagida: Mechanochemical coupling in actomyosin energy transduction studied by *in vitro* movement assay. *J Mol Biol* 216, 49-68. (1990)
33. E Homsher, F Wang, JR Sellers: Factors affecting movement of F-actin filaments propelled by skeletal muscle heavy meromyosin. *Am J Physiol* 262, C714-23. (1992)
34. M Sundberg, M Balaz, R Bunk, JP Rosengren-Holmberg, L Montelius, IA Nicholls, P Omling, S Tagerud, A Mansson: Selective spatial localization of actomyosin motor function by chemical surface patterning. *Langmuir* 22, 7302-12 (2006)
35. A Kishino, T Yanagida: Force Measurements by Micromanipulation of a Single Actin Filament by Glass Needles. *Nature* 334, 74-76 (1988)
36. JE Molloy, JE Burns, J Kendrick-Jones, RT Tregear, DC White: Movement and force produced by a single myosin head. *Nature* 378, 209-12 (1995)
37. C Ruegg, C Veigel, JE Molloy, S Schmitz, JC Sparrow, RHA Fink: Molecular motors: Force and movement generated by single myosin II molecules. *News Physiol Sci* 17, 213-218 (2002)
38. F Vanzi, M Capitanio, L Sacconi, C Stringari, R Cicchi, M Canepari, M Maffei, N Piroddi, C Poggesi, V Nucciotti, M Linari, G Piazzesi, C Tesi, R Antolini, V Lombardi, R Bottinelli, FS Pavone: New techniques in linear and non-linear laser optics in muscle research. *J Muscle Res Cell Motil* 27, 469-479 (2006)
39. M Capitanio, M Canepari, P Cacciafesta, V Lombardi, R Cicchi, M Maffei, FS Pavone, R Bottinelli: Two independent mechanical events in the interaction cycle of skeletal muscle myosin with actin. *Proc Natl Acad Sci U S A* 103, 87-92 (2006)
40. W Steffen, D Smith, R Simmons, J Sleep: Mapping the actin filament with myosin. *Proc Natl Acad Sci U S A* 98, 14949-14954 (2001)
41. MJ Tyska, DE Dupuis, WH Guilford, JB Patlak, GS Waller, KM Trybus, DM Warshaw, S Lowey: Two heads of myosin are better than one for generating force and motion. *Proc Natl Acad Sci U S A* 96, 4402-7 (1999)
42. C Veigel, LM Coluccio, JD Jontes, JC Sparrow, RA Milligan, JE Molloy: The motor protein myosin-I produces its working stroke in two steps. *Nature* 398, 530-3 (1999)
43. Y Takagi, EE Homsher, YE Goldman, H Shuman: Force generation in single conventional actomyosin complexes under high dynamic load. *Biophys J* 90, 1295-307 (2006)
44. C Ruff, M Furch, B Brenner, DJ Manstein, E Meyhofer: Single-molecule tracking of myosins with genetically engineered amplifier domains. *Nat Struct Biol* 8, 226-229 (2001)
45. H Tanaka, A Ishijima, M Honda, K Saito, T Yanagida: Orientation dependence of displacements by a single one-headed myosin relative to the actin filament. *Biophys J* 75, 1886-94 (1998)
46. S Marston: Random walks with thin filaments: application of *in vitro* motility assay to the study of actomyosin regulation. *J Muscle Res Cell Motil* 24, 149-156 (2003)
47. MG van den Heuvel, C Dekker: Motor proteins at work for nanotechnology. *Science* 317, 333-6 (2007)
48. JE Molloy: Muscle contraction: actin filaments enter the fray. *Biophys J* 89, 1-2 (2005)
49. T Scholz, B Brenner: Actin sliding on reconstituted myosin filaments containing only one myosin heavy chain isoform. *J Muscle Res Cell Motil* 24, 77-86 (2003)
50. E Thedinga, N Karim, T Kraft, B Brenner: A single-fiber *in vitro* motility assay. *In vitro* sliding velocity of F- actin vs. unloaded shortening velocity in skinned muscle fibers. *J Muscle Res Cell Motil* 20, 785-96. (1999)
51. M Canepari, R Rossi, MA Pellegrino, C Reggiani, R Bottinelli: Speeds of actin translocation *in vitro* by myosins extracted from single rat muscle fibres of different types. *Exp Physiol* 84, 803-6 (1999)

52. P Hook, L Larsson: Actomyosin interactions in a novel single muscle fiber *in vitro* motility assay. *J Muscle Res Cell Motil* 21, 357-65. (2000)
53. I Rayment, HM Holden, M Whittaker, CB Yohn, M Lorenz, KC Holmes, RA Milligan: Structure of the actin-myosin complex and its implications for muscle contraction. *Science* 261, 58-65 (1993)
54. A Houdusse, AG Szent-Gyorgyi, C Cohen: Three conformational states of scallop myosin S1. *Proc Natl Acad Sci U S A* 97, 11238-43. (2000)
55. M Reconditi, M Linari, L Lucii, A Stewart, YB Sun, P Boesecke, T Narayanan, RF Fischetti, T Irving, G Piazzesi, M Irving, V Lombardi: The myosin motor in muscle generates a smaller and slower working stroke at higher load. *Nature* 428, 578-581 (2004)
56. A Yamada, M Yoshio, H Nakayama: Bi-directional movement of actin filaments along long bipolar tracks of oriented rabbit skeletal muscle myosin molecules. *FEBS Lett* 409, 380-4 (1997)
57. AM Gordon, E Homsher, M Regnier: Regulation of contraction in striated muscle. *Physiol Rev* 80, 853-924. (2000)
58. S Fujita-Becker, U Durrwang, M Erent, RJ Clark, MA Geeves, DJ Manstein: Changes in Mg2+ ion concentration and heavy chain phosphorylation regulate the motor activity of a class I myosin. *J Biol Chem* 280, 6064-71 (2005)
59. AP Minton: The influence of macromolecular crowding and macromolecular confinement on biochemical reactions in physiological media. *J Biol Chem* 276, 10577-80 (2001)
60. J Sleep, A Lewalle, D Smith: Reconciling the working strokes of a single head of skeletal muscle myosin estimated from laser-trap experiments and crystal structures. *Proc Natl Acad Sci U S A* 103, 1278-1282 (2006)
61. A Mansson, S Tagerud: Multivariate statistics in analysis of data from the *in vitro* motility assay. *Anal Biochem* 314, 281-93 (2003)
62. W Bing, ID Fraser, SB Marston: Troponin I and troponin T interact with troponin C to produce different Ca2+-dependent effects on actin-tropomyosin filament motility. *Biochem J* 327, 335-40 (1997)
63. JJ Ramsden, DJ Roush, DS Gill, R Kurrat, RC Willson: Protein Adsorption-Kinetics Drastically Altered by Repositioning a Single Charge. *J Am Chem Soc* 117, 8511-8516 (1995)
64. CM Roth, AM Lenhoff: Electrostatic and Vanderwaals Contributions to Protein Adsorption - Computation of Equilibrium-Constants. *Langmuir* 9, 962-972 (1993)
65. JA Redman, SL Walker, M Elimelech: Bacterial adhesion and transport in porous media: Role of the secondary energy minimum. *Environ Sci Technol* 38, 1777-1785 (2004)
66. RA Milligan: Protein-protein interactions in the rigor actomyosin complex. *Proc Natl Acad Sci U S A* 93, 21-26 (1996)
67. J Gulati, RJ Podolsky: Isotonic contraction of skinned muscle fibers on a slow time base: effects of ionic strength and calcium. *J Gen Physiol* 78, 233-57 (1981)
68. FGD Banos, J Bordas, J Lowy, A Svensson: Small Segmental Rearrangements in the Myosin Head Can Explain Force Generation in Muscle. *Biophys J* 71, 576-589 (1996)
69. S Highsmith: Electrostatic Contributions to the Binding of Myosin and Myosin-MgADP to F-Actin in Solution. *Biochemistry* 29, 10690-10694 (1990)
70. CT Murphy, JA Spudich: The sequence of the myosin 50-20K loop affects Myosin's affinity for actin throughout the actin-myosin ATPase cycle and its maximum ATPase activity. *Biochemistry* 38, 3785-92 (1999)
71. AR Hodges, EB Krementsova, KM Trybus: Engineering the processive run length of Myosin v. *J Biol Chem* 282, 27192-7 (2007)
72. SF Chen, LY Liu, J Zhou, SY Jiang: Controlling antibody orientation on charged self-assembled monolayers. *Langmuir* 19, 2859-2864 (2003)
73. J Zhou, SF Chen, SY Jiang: Orientation of adsorbed antibodies on charged surfaces by computer simulation based on a united-residue model. *Langmuir* 19, 3472-3478 (2003)
74. H Wang, DG Castner, BD Ratner, SY Jiang: Probing the orientation of surface-immobilized immunoglobulin G by time-of-flight secondary ion mass spectrometry. *Langmuir* 20, 1877-1887 (2004)
75. CF Wertz, MM Santore: Effect of surface hydrophobicity on adsorption and relaxation kinetics of albumin and fibrinogen: Single-species and competitive behavior. *Langmuir* 17, 3006-3016 (2001)
76. J Buijs, DW Britt, V Hlady: Human growth hormone adsorption kinetics and conformation on self-assembled monolayers. *Langmuir* 14, 335-341 (1998)
77. M van der Veen, MC Stuart, W Norde: Spreading of proteins and its effect on adsorption and desorption kinetics. *Colloids and Surfaces B-Biointerfaces* 54, 136-142 (2007)
78. AP Minton: Adsorption of globular proteins on locally planar surfaces. II. Models for the effect of multiple adsorbate conformations on adsorption equilibria and kinetics. *Biophys J* 76, 176-187 (1999)
79. H Nygren: Nonlinear Kinetics of Ferritin Adsorption. *Biophys J* 65, 1508-1512 (1993)
80. C Calonder, Y Tie, PR Van Tassel: History dependence of protein adsorption kinetics. *Proc Natl Acad Sci U S A* 98, 10664-10669 (2001)
81. SS Margossian, S Lowey: Preparation of myosin and its subfragments from rabbit skeletal muscle. *Methods Enzymol* 85, 55-71 (1982)
82. RC Lu: Identification of a Region Susceptible to Proteolysis in Myosin Subfragment-2. *Proc Natl Acad Sci U S A* 77, 2010-2013 (1980)
83. RC Lu, A Wong: The Amino-Acid Sequence and Stability Predictions of the Hinge Region in Myosin Subfragment-2. *J Biol Chem* 260, 3456-3461 (1985)
84. M Walker, J Trinick: Electron microscope study of the effect of temperature on the length of the tail of the myosin molecule. *J Mol Biol* 192, 661-7 (1986)
85. D Gundapaneni, J Xu, DD Root: High flexibility of the actomyosin crossbridge resides in skeletal muscle myosin subfragment-2 as demonstrated by a new single molecule assay. *J Struct Biol* 149, 117-126 (2005)
86. W Blankenfeldt, NH Thoma, JS Wray, M Gautel, I Schlichting: Crystal structures of human cardiac beta-myosin II S2-Delta provide insight into the functional role

of the S2 subfragment. *Proc Natl Acad Sci U S A* 103, 17713-7 (2006)
87. T Aoki, Y Sowa, H Yokota, M Hiroshima, M Tokunaga, Y Ishii, T Yanagida: Non-contact electrostatic surface force imaging of single protein filaments using intermolecular force microscopy. *Single Molecules* 2, 183-190 (2001)
88. S Hvidt, FHM Nestler, ML Greaser, JD Ferry: Flexibility of Myosin Rod Determined from Dilute-Solution Viscoelastic Measurements. *Biochemistry* 21, 4064-4073 (1982)
89. PJ Knight: Dynamic behaviour of the head-tail junction of myosin. *J Mol Biol* 255, 269-74. (1996)
90. G Offer, P Knight: The structure of the head-tail junction of the myosin molecule. *J Mol Biol* 256, 407-416 (1996)
91. I Rayment, WR Rypniewski, K Schmidt-Base, R Smith, DR Tomchick, MM Benning, DA Winkelmann, G Wesenberg, HM Holden: Three-dimensional structure of myosin subfragment-1: a molecular motor. *Science* 261, 50-8 (1993)
92. K Guruprasad, BVB Reddy, MW Pandit: Correlation between Stability of a Protein and Its Dipeptide Composition - a Novel-Approach for Predicting Invivo Stability of a Protein from Its Primary Sequence. *Protein Eng* 4, 155-161 (1990)
93. JW Shriver, U Kamath: Differential Scanning Calorimetry of the Unfolding of Myosin Subfragment-1, Subfragment-2, and Heavy-Meromyosin. *Biochemistry* 29, 2556-2564 (1990)
94. A Michnik, K Michalik, Z Drzazga: Stability of bovine serum albumin at different pH. *J Therm Anal Calorimetry* 80, 399-406 (2005)
95. M Burke, S Zaager, J Bliss: Substructure of Skeletal Myosin Subfragment-1 Revealed by Thermal-Denaturation. *Biochemistry* 26, 1492-1496 (1987)
96. M Burke, M Sivaramakrishnan: Substructure of Skeletal Myosin Subfragment-1 - Preferential Destabilization of a Domain by Methanol and Its Effect on Catalytic Activity. *J Biol Chem* 261, 2330-2336 (1986)
97. TQP Uyeda, KM Ruppel, JA Spudich: Enzymatic-Activities Correlate with Chimeric Substitutions at the Actin-Binding Face of Myosin. *Nature* 368, 567-569 (1994)
98. CM Yengo, HL Sweeney: Functional role of loop 2 in myosin V. *Biochemistry* 43, 2605-2612 (2004)
99. RR Thomas, FB Kaufman, JT Kirleis, RA Belsky: Wettability of polished silicon oxide surfaces. *J Electrochem Soc* 143, 643-648 (1996)
100. H Suzuki, A Yamada, K Oiwa, H Nakayama, S Mashiko: Control of actin moving trajectory by patterned poly (methylmethacrylate) tracks. *Biophys J* 72, 1997-2001 (1997)
101. DV Nicolau, H Suzuki, S Mashiko, T Taguchi, S Yoshikawa: Actin motion on microlithographically functionalized myosin surfaces and tracks. *Biophys J* 77, 1126-1134 (1999)
102. R Bunk, J Klinth, L Montelius, IA Nicholls, P Omling, S Tagerud, A Mansson: Actomyosin motility on nanostructured surfaces. *Biochem Biophys Res Commun* 301, 783-8 (2003)
103. M Sundberg, JP Rosengren, R Bunk, J Lindahl, IA Nicholls, S Tagerud, P Omling, L Montelius, A Mansson: Silanized surfaces for *in vitro* studies of actomyosin function and nanotechnology applications. *Anal Biochem* 323, 127-38 (2003)
104. M Sundberg, R Bunk, N Albet-Torres, A Kvennefors, F Persson, L Montelius, IA Nicholls, S Ghatnekar-Nilsson, P Omling, S Tagerud, A Mansson: Actin Filament Guidance on a Chip: Toward High-Throughput Assays and Lab-on-a-Chip Applications. *Langmuir* 22, 7286-95 (2006)
105. IVM Barbosa, DM Merquior, FC Peixoto: Continuous modelling and kinetic parameter estimation for cellulose nitration. *Chem Eng Sci* 60, 5406-5413 (2005)
106. A Mansson, J Klinth, E Johansson-Karlsson, C Widén, J Johnsson, L Montelius: Scanning probe microscopy study of myosin binding, topography and elastic properties of thin nitrocellulose films. *Biophys J* 80, 77a (2001)
107. E Katayama: Quick-freeze deep-etch electron microscopy of the actin-heavy meromyosin complex during the *in vitro* motility assay. *J Mol Biol* 278, 349-67 (1998)
108. P Hallett, G Offer, MJ Miles: Atomic force microscopy of the myosin molecule. *Biophys J* 68, 1604-6 (1995)
109. S Sheng, Y Gao, AS Khromov, AV Somlyo, AP Somlyo, Z Shao: Cryo-atomic force microscopy of unphosphorylated and thiophosphorylated single smooth muscle myosin molecules. *J Biol Chem* 278, 39892-6 (2003)
110. T Ando, N Kodera, E Takai, D Maruyama, K Saito, A Toda: A high-speed atomic force microscope for studying biological macromolecules. *Proc Natl Acad Sci U S A* 98, 12468-72. (2001)
111. R Bunk, M Sundberg, IA Nicholls, P Omling, S Tågerud, A Månsson, L Montelius: Guiding motor-propelled molecules with nanoscale precision through silanized bi-channel structures. *Nanotechnol* 16, 710-717 (2005)
112. M Balaz, M Sundberg, M Persson, J Kvassman, A Mansson: Effects of Surface Adsorption on Catalytic Activity of Heavy Meromyosin Studied using Fluorescent ATP Analogue. *Biochemistry* 46, 7233-7251 (2007)
113. JA Jaber, PB Chase, JB Schlenoff: Actomyosin-driven motility on patterned polyelectrolyte mono- and multilayers. *Nano Letters* 3, 1505-1509 (2003)
114. DV Nicolau, G Solana, M Kekic, F Fulga, C Mahanivong, J Wright, C dos Remedios: Surface hydrophobicity modulates the operation of actomyosin-based dynamic nanodevices. *Langmuir* 23, 10846-10854 (2007)
115. TQ Uyeda, SJ Kron, JA Spudich: Myosin step size. Estimation from slow sliding movement of actin over low densities of heavy meromyosin. *J Mol Biol* 214, 699-710 (1990)
116. YY Toyoshima, SJ Kron, JA Spudich: The myosin step size: measurement of the unit displacement per ATP hydrolyzed in an *in vitro* assay. *Proc Natl Acad Sci U S A* 87, 7130-4 (1990)
117. H Komatsu, T Kanno, Y Matsumoto, T Kodama: Alcohol-induced biphasic inhibition of myosin subfragment 1 K-EDTA-ATPase. *Biochim Biophys Acta-Prot Struct Mol Enzymol* 1430, 14-24 (1999)

118. WW Kielley, HM Kalckar, LB Bradley: The hydrolysis of purine and pyrimidine nucleoside triphosphates by myosin. *J Biol Chem* 219, 95-101 (1956)
119. YY Toyoshima: How are myosin fragments bound to nitrocellulose film? *Adv Exp Med Biol* 332, 259-65 (1993)
120. B Guo, WH Guilford: The tail of myosin reduces actin filament velocity in the *in vitro* motility assay. *Cell Motil Cytoskeleton* 59, 264-72 (2004)
121. DE Harris, DM Warshaw: Smooth and skeletal muscle myosin both exhibit low duty cycles at zero load *in vitro*. *J Biol Chem* 268, 14764-8. (1993)
122. B Lassen, M Malmsten: Competitive protein adsorption studied with TIRF and ellipsometry. *J Colloid Interface Sci* 179, 470-477 (1996)
123. D Axelrod: Total internal reflection fluorescence microscopy in cell biology. *Methods Enzymol* 361, 1-33 (2003)
124. R Cardinaud, JC Bernengo: Electric birefringence study of rabbit skeletal myosin subfragments HMM, LMM, and rod in solution. *Biophys J* 48, 751-63 (1985)
125. H Hayashi, K Takiguchi, S Higashi-Fujime: Measurement of ATPase activity of immobilized myosin heads. *J Biochem (Tokyo)* 105, 875-7 (1989)
126. S Highsmith, K Duignan, K Franks-Skiba, K Polosukhina, R Cooke: Reversible inactivation of myosin subfragment 1 activity by mechanical immobilization. *Biophys J* 74, 1465-72 (1998)
127. CK O'Sullivan, GG Guilbault: Commercial quartz crystal microbalances - theory and applications. *Biosensors & Bioelectronics* 14, 663-670 (1999)
128. A Janshoff, HJ Galla, C Steinem: Piezoelectric mass-sensing devices as biosensors - An alternative to optical biosensors? *Angew Chemie-Int Ed* 39, 4004-4032 (2000)
129. MA Cooper, VT Singleton: A survey of the 2001 to 2005 quartz crystal microbalance biosensor literature: applications of acoustic physics to the analysis of biomolecular interactions. *J Mol Rec* 20, 154-184 (2007)
130. G Sauerbrey: Verwendung Von Schwingquarzen Zur Wagung Dunner Schichten Und Zur Mikrowagung. *Zeitschrift Fur Physik* 155, 206-222 (1959)
131. F Hook, B Kasemo, T Nylander, C Fant, K Sott, H Elwing: Variations in coupled water, viscoelastic properties, and film thickness of a Mefp-1 protein film during adsorption and cross-linking: A quartz crystal microbalance with dissipation monitoring, ellipsometry, and surface plasmon resonance study. *Anal Chem* 73, 5796-5804 (2001)
132. M Malmsten, B Lassen, K Holmberg, V Thomas, G Quash: Effects of hydrophilization and immobilization on the interfacial behavior of immunoglobulins. *J Colloid Interface Sci* 177, 70-78 (1996)
133. S Pasche, M Textor, L Meagher, ND Spencer, HJ Griesser: Relationship between interfacial forces measured by colloid-probe atomic force microscopy and protein resistance of poly (ethylene glycol)-grafted poly (L-lysine) adlayers on niobia surfaces. *Langmuir* 21, 6508-6520 (2005)
134. D Falconnet, D Pasqui, S Park, R Eckert, H Schift, J Gobrecht, R Barbucci, M Textor: A novel approach to produce protein nanopatterns by combining nanoimprint lithography and molecular self-assembly. *Nano Letters* 4, 1909-1914 (2004)
135. R Rosario, D Gust, M Hayes, F Jahnke, J Springer, AA Garcia: Photon-modulated wettability changes on spiropyran-coated surfaces. *Langmuir* 18, 8062-8069 (2002)
136. GB Sigal, M Mrksich, GM Whitesides: Effect of surface wettability on the adsorption of proteins and detergents. *J Am Chem Soc* 120, 3464-3473 (1998)
137. PB Conibear, MA Geeves: Cooperativity between the two heads of rabbit skeletal muscle heavy meromyosin in binding to actin. *Biophys J* 75, 926-37 (1998)
138. KA.P. Edman, A Mansson, C Caputo: The biphasic force-velocity relationship in frog muscle fibres and its evaluation in terms of cross-bridge function (published erratum appears in J Physiol (Lond) 1997 Nov 1;504 (Pt 3):763). *J Physiol (Lond)* 503, 141-56 (1997)
139. AF Huxley, S Tideswell: Rapid regeneration of power stroke in contracting muscle by attachment of second myosin head. *J Muscle Res Cell Motil* 18, 111-4 (1997)
140. JA Trinick, G Offer: Cross-linking of actin filaments by heavy meromyosin. *J. Mol. Biol.* 133, 549-556 (1979)
141. N Jalili, K Laxminarayana: A review of atomic force microscopy imaging systems: application to molecular metrology and biological sciences. *Mechatronics* 14, 907-945 (2004)
142. P Hinterdorfer, YF Dufrene: Detection and localization of single molecular recognition events using atomic force microscopy. *Nat Methods* 3, 347-355 (2006)
143. K Merrett, RM Cornelius, WG McClung, LD Unsworth, H Sheardown: Surface analysis methods for characterizing polymeric biomaterials. *J Biomat Sci-Polymer Ed* 13, 593-621 (2002)
144. DY Kwok, AW Neumann: Contact angle measurement and contact angle interpretation. *Adv Colloid Interface Sci* 81, 167-249 (1999)
145. M Sundberg, A Mansson, S Tagerud: Contact angle measurements by confocal microscopy for non-destructive microscale surface characterization. *J Colloid Interface Sci* 313, 454-60 (2007)
146. S Jo, K Park: Surface modification using silanated poly (ethylene glycol)s. *Biomaterials* 21, 605-16. (2000)
147. Y Yokoyama, R Ishiguro, H Maeda, M Mukaiyama, K Kameyama, K Hiramatsu: Quantitative analysis of protein adsorption on a planar surface by Fourier transform infrared spectroscopy: lysozyme adsorbed on hydrophobic silicon-containing polymer. *J Colloid Interface Sci* 268, 23-32 (2003)
148. JR Lu, XB Zhao, M Yaseen: Protein adsorption studied by neutron reflection. *Curr Opin Colloid Interface Sci* 12, 9-16 (2007)
149. H Elwing: Protein absorption and ellipsometry in biomaterial research. *Biomaterials* 19, 397-406 (1998)
150. J Buijs, V Hlady: Adsorption kinetics, conformation, and mobility of the growth hormone and lysozyme on solid surfaces, studied with TIRF. *J Colloid Interface Sci* 190, 171-181 (1997)
151. R Karlsson: SPR for molecular interaction analysis: a review of emerging application areas. *J Mol Rec* 17, 151-61 (2004)
152. C Boozer, G Kim, SX Cong, HW Guan, T Londergan: Looking towards label-free biomolecular interaction analysis in a high-throughput format: a review of new

surface plasmon resonance technologies. *Curr Opin Biotechnol* 17, 400-405 (2006)
153. F Hook, J Voros, M Rodahl, R Kurrat, P Boni, JJ Ramsden, M Textor, ND Spencer, P Tengvall, J Gold, B Kasemo: A comparative study of protein adsorption on titanium oxide surfaces using *in situ* ellipsometry, optical waveguide lightmode spectroscopy, and quartz crystal microbalance/dissipation. *Colloids and Surfaces B-Biointerfaces* 24, 155-170 (2002)
154. A Janshoff, HJ Galla, C Steinem: Piezoelectric Mass-Sensing Devices as Biosensors-An Alternative to Optical Biosensors? *Angew Chem Int Ed Engl* 39, 4004-4032 (2000)
155. KL Hanson, V Viidyanathan, DV Nicolau: Actomyosin motility detection using quartz crystal microbalance. *Proc SPIE* Vol. 6036, 1-8 (2006)
156. BJ Kirby, EF Hasselbrink: Zeta potential of microfluidic substrates: 1. Theory, experimental techniques, and effects on separations. *Electrophoresis* 25, 187-202 (2004)
157. T Yanagida, M Nakase, K Nishiyama, F Oosawa: Direct observation of motion of single F-actin filaments in the presence of myosin. *Nature* 307, 58-60 (1984)
158. YY Toyoshima, SJ Kron, EM McNally, KR Niebling, C Toyoshima, JA Spudich: Myosin subfragment-1 is sufficient to move actin filaments *in vitro*. *Nature* 328, 536-9 (1987)
159. Y Harada, A Noguchi, A Kishino, T Yanagida: Sliding Movement of Single Actin-Filaments on One-Headed Myosin-Filaments. *Nature* 326, 805-808 (1987)
160. YY Toyoshima, C Toyoshima, JA Spudich: Bidirectional movement of actin filaments along tracks of myosin heads. *Nature* 341, 154-6 (1989)
161. TQ Uyeda, HM Warrick, SJ Kron, JA Spudich: Quantized velocities at low myosin densities in an *in vitro* motility assay. *Nature* 352, 307-11. (1991)
162. T Nishizaka, T Yagi, Y Tanaka, S Ishiwata: Right-handed rotation of an actin filament in an *in vitro* motile system. *Nature* 361, 269-71 (1993)
163. N Suzuki, H Miyata, S Ishiwata, K Kinosita, Jr.: Preparation of bead-tailed actin filaments: estimation of the torque produced by the sliding force in an *in vitro* motility assay. *Biophys J* 70, 401-8 (1996)
164. E Homsher, B Kim, A Bobkova, LS Tobacman: Calcium regulation of thin filament movement in an *in vitro* motility assay. *Biophys J* 70, 1881-92 (1996)
165. C Veigel, JE Molloy, S Schmitz, J Kendrick-Jones: Load-dependent kinetics of force production by smooth muscle myosin measured with optical tweezers. *Nature Cell Biology* 5, 980-986 (2003)
166. G Tsiavaliaris, S Fujita-Becker, DJ Manstein: Molecular engineering of a backwards-moving myosin motor. *Nature* 427, 558-561 (2004)
167. D Eden, S Highsmith: Light chain-dependent myosin structural dynamics in solution investigated by transient electrical birefringence. *Biophys J* 73, 952-958 (1997)
168. A Lambacher, P Fromherz: Luminescence of dye molecules on oxidized silicon and fluorescence interference contrast microscopy of biomembranes. *J Opt Soc Am B-Opt Phys* 19, 1435 (2002)
169. R Koradi, M Billeter, K Wuthrich: MOLMOL: a program for display and analysis of macromolecular structures. *J Mol Graph* 14, 51-5, 29-32 (1996)

**Abbreviations:** Alexa-ATP: Adenosine 5'-triphosphate Alexa Fluor® 647 2'- (or 3')-O- (N- (2-aminoethyl)urethane), hexa (triethylammonium) salt; ADP: Adenosine 5'-diphosphate; ATP: Adenosine 5'-triphosphate; ATPase: Adenosine 5'-triphosphatase; BSA: bovine serum albumin; ELC, Essential light chain; HMM, Heavy meromyosin; HPLC, High pressure liquid chromatography; IVMA: *in vitro* motility assay; PEG, Poly ethylene glycol; RLC, Regulatory light chain; QCM, Quartz crystal microbalance; S1, Subfragment 1; S2, Subfragment 2; SDS-PAGE, Sodium dodecyl sulphate polyacrylamide gel electrophoresis; SEM, Standard error of the mean; T, Temperature; TIR, Total internal reflection; TIRF, Total internal reflection fluorescence; TMCS, Trimethylchlorosilane

**Key Words** Heavy meromoysin, *In vitro* motility assay, Actomyosin, Adsorption, Review

**Send correspondence to***:* Alf Mansson, School of Pure and Applied Natural Sciences, University of Kalmar, SE-391 82 Kalmar, Sweden, Tel: 46 480-446243, Fax: 46 -480 -446262, E-mail: alf.mansson@hik.se

**http://www.bioscience.org/current/vol13.htm**